



Influence of lipid membranes on huntingtin exon 1 fibrillation

Daniela Muntean

Thesis to obtain the Master of Science Degree in
Biotechnology

Supervisors:

Dr. Ana Margarida Pereira de Melo
Dr. Ana Margarida Nunes da Mata Pires de Azevedo

Examination Committee:

Chairperson: Prof. Arsénio do Carmo Sales Mendes Fialho
Supervisor: Dr. Ana Margarida Pereira de Melo
Members of the Committee: Dr. Ana Isabel Abrantes Coutinho

October 2022

Preface

This thesis has the objective of describing the biophysical properties of Httex1, namely the formation of aggregates or fibrils on the Httex1 containing 37 runs of glutamine (Httex1-37Q) as well as 43 runs of glutamine (Httex1-43Q).

Declaration

I declare that this document is an original work of my own authorship and that it fulfils all the requirements of the Code of Conduct and Good Practices of the Universidade de Lisboa.

Acknowledgements

I would first like to thank my supervisor, PhD Ana Melo and my co-supervisor PhD Ana Azevedo, for the support and guidance she has given me during the past year. Big thanks to the host laboratory for allowing me to work on this amazing and challenging project. I will be forever grateful for the patience and availability given to me. I would also like to thank PhD Cláudia Alves for all the time she spent guiding and teaching me. I won't forget to also thank Jorge João and Sara Rosa in the lab at South Tower for helping me and tutoring me when I reached out for their help.

Next, I want to thank my parents for all the effort they put into my education. Thank you for all the hours and extra hours you worked for my sake, for the support given and allowing me to pursue my interests, both scientific and artistic. Thank you, mom and dad, for the time you spent listening to me, my dreams, and my plans.

To my closest friends Constança, Sofia, and Madalena, thank you. Having you listen and keep me company in the hardest moments helped me push through and do my best. Big thanks to all of my friends that I wasn't able to spend as much time with, but still supported me nonetheless. And of course, to all the amazing people I met during my journey in the lab, thank you for keeping me company; thank you Gonçalo, Diogo, Adriana, Nuno, Ricardo and many others. Special thanks to Ricardo for writing a life-saving script, I owe you this one.

If I were to name everyone that helped through this journey, I would need a lifetime and a half. Each one of you, no matter how ephemeral our contact, plays a piece in this project. To all of you, I appreciate the encouragement.

Abstract

Huntington's disease (HD) is an inherited neurodegenerative disorder caused by a CAG repeat expansion within the first exon of the huntingtin (HTT) gene. Pathological extensions above a critical threshold of 37 CAG lead to an expression of a mutant huntingtin (Htt) protein comprising an expanded polyglutamine (polyQ) domain. The aberrant splicing and proteolytic cleavage of mutant Htt proteins result in highly toxic Htt fragments spanning exon 1 (Httex1), which are sufficient to reproduce most of HD's pathology. Recent studies support that biological membranes promote Httex1 misfolding and aggregation. This project aims to establish an approach for studying the amyloid fiber formation of Httex1 and to evaluate the impact of anionic lipid membranes. The aggregation of Httex1-37Q and Httex1-43Q variants were here evaluated by ThT fluorescence assays. Initially, a strategy for production of tag-free Httex1-37Q was developed using a solubilizing SUMO-fusion approach. However, ThT fluorescence assays revealed that tag-free Httex1-37Q was already aggregated before starting the assay. Instead, the mutant Httex1-43Q variant was purified as a fusion construct and the SUMO-tag was only removed during the ThT assay. Remarkably, tag-cleavage is almost instantly avoiding interference on the assay. The fibrillation kinetics of Httex1-43Q show a typical sigmoid curve profile and that anionic lipid membranes potentiate its fibrillation, in accordance with current literature data. Our approach provides an excellent platform for studying Httex1 amyloid fibril formation in solution and in the presence of lipid membranes, allowing to investigate different variants, concentrations, and lipid compositions.

Keywords

httex1, fibrillation, kinetics, lipid, Thioflavin-T

Resumo

A Doença de Huntington (HD) é uma doença herdada neurodegenerativa causada pela expansão da repetição CAG no primeiro exão do gene da *huntingtin* (*HTT*). Expansões patológicas acima de um *threshold* 37 CAG levam à expressão da proteína huntingtin mutante (Htt) contendo um domínio poliglutamina (Q) expandido. O *splicing* aberrante e clivagem proteolítica das proteínas Htt mutantes resultam num fragmento altamente tóxico da Htt que engloba o exão 1 (Httex1), que é suficiente para reproduzir a HD. Estudos recentes apoiam que membranas biológicas promovem a agregação do Httex1. O objetivo deste projeto é estabelecer um protocolo para estudar a formação de fibras amiloides da Httex1 e avaliar o impacto de membranas lipídicas aniónicas. A agregação das variantes Httex1-37Q e Httex1-43Q foram avaliadas por ensaios de fluorescência com ThT. Inicialmente, a estratégia envolveu a produção de *tag-free* Httex1-37Q usando a SUMO-tag para solubilização. O ensaio de fluorescência com ThT revelou que a *tag-free* Httex1-37Q já estava agregada antes do início do ensaio. Portanto, a variante mutante Httex1-43Q foi purificada como proteína de fusão e o SUMO-tag só foi removido durante o ensaio ThT. A clivagem do tag é quase instantânea, evitando interferência no ensaio. A cinética de fibrilação da Httex1-43Q mostra o perfil de uma curva sigmoide e que as membranas lipídicas aniónicas potenciam a fibrilação, de acordo com literatura corrente. O nosso protocolo permite uma plataforma excelente para estudar a formação de fibras amiloides Httex1 em solução e na presença de membranas lipídicas, permitindo investigar diferentes variantes, concentrações, e composições lipídicas.

Palavras-chave

httex1, fibrilação, cinética, lípido, Thioflavin-T

Table of Contents

| | |
|--|------|
| Preface..... | III |
| Declaration | V |
| Acknowledgements..... | VII |
| Abstract | IX |
| Resumo | XI |
| List of Tables | XV |
| List of Figures | XVII |
| List of Abbreviations..... | XIX |
| CHAPTER 1 <i>INTRODUCTION</i> | XXI |
| 1.1 Neurodegenerative diseases and protein aggregation..... | 1 |
| 1.2 Formation of amyloid fibers and detection methods | 2 |
| 1.3 Huntington’s Disease (HD) | 6 |
| 1.4 Symptoms, diagnosis and treatment..... | 6 |
| 1.5 Huntingtin protein (Htt) | 7 |
| 1.6 Huntingtin exon 1 (Httex1) | 8 |
| 1.7 Recombinant Expression and purification of Httex1 | 11 |
| 1.8 Kinetics and lipids..... | 13 |
| Goals and work-plan | 16 |
| CHAPTER 2 <i>MATERIALS AND METHODS</i> | 17 |
| 2.1 Plasmids, bacterial strains, materials and chemicals..... | 19 |
| 2.2 Site-directed mutagenesis of pET-SUMO-Httex1-37Q..... | 19 |
| 2.3. Production of tag-free Httex1-37Q | 20 |
| 2.3.1 Expression test and large scale expression of His6-SUMO-Httex1-37Q | 20 |
| 2.3.2. Purification of tag-free Httex1-37Q protein | 21 |
| 2.4. Production of the His6-SUMO-Httex1-43Q fusion protein | 22 |
| 2.5 SDS-PAGE gels | 23 |
| 2.6 Liposome Preparation | 23 |
| 2.7 ThT fluorescence assays..... | 23 |

| | |
|--|----|
| CHAPTER 3 <i>RESULTS AND DISCUSSION</i> | 25 |
| 3.1. Production of tag-free Httex1-37Q | 27 |
| 3.1.1. Expression test of His6-SUMO-Httex1-37Q..... | 27 |
| 3.1.2. Purification of the tag-free Httex1-37Q | 27 |
| 3.2. ThT fluorescence assays of tag-free Httex1-37Q | 31 |
| 3.3. Production of the His ₆ -SUMO-Httex1-43Q fusion protein..... | 34 |
| 3.4. ThT fluorescence assays of Httex1-43Q | 35 |
| 3.4.1. Fibrillation of Httex1-43Q in solution..... | 35 |
| 3.4.2. Fibrillation of His6-SUMO-Httex1-43Q with lipid vesicles | 38 |
| 3.5. Discussion..... | 42 |
| CHAPTER 4 <i>CONCLUSION</i> | 45 |
| 4. Conclusion | 47 |
| 4.1. Further Studies..... | 47 |
| Bibliography | 48 |

List of Tables

| | |
|---|----|
| Table 1.1. A selection of human diseases where the formation of protein amyloid aggregates is an important feature and their respective pathological proteins. | 1 |
| Table 1.2. Table containing a list of the most common Httex1 fusion proteins and proteases used for in vitro aggregation studies. | 11 |
| Table 2.1. Sequence of the primers used for site-directed mutagenesis. | 20 |
| Table 3.1. Average (mean) and standard deviation (STDEV) of ThT fluorescence intensities upon incubation with tag-free Httex1-37Q for the data presented in Figure 3.3 (for ~ 16 hours). | 31 |
| Table 3.2. ThT fluorescence intensity values registered at 29, 52, and 196 hours after starting the aggregation kinetic assay. | 31 |
| Table 3.3. Average (mean) and standard deviation (STDEV) of ThT fluorescence intensities obtained upon incubation with tag-free Httex1-43Q for the data presented in Figure 3.5 (for ~ 16 hours). | 34 |

List of Figures

| | |
|--|----|
| Figure 1.1. Schematic representation of the energy landscape for protein folding and aggregation. | 2 |
| Figure 1.2. General aggregation profile of proteins that follow a nucleation-polymerization pathway for amyloid fiber formation. | 3 |
| Figure 1.3. Chemical structure of Thioflavin-T (ThT). | 4 |
| Figure 1.4. Schematic representation of cross- β amyloid structures. | 5 |
| Figure 1.5. Schematic representation of several features of Htt. | 7 |
| Figure 1.6. The proposed mechanism for the incomplete splicing and proteolysis. | 9 |
| Figure 1.7. The proposed model for polyQ aggregate nucleation and extension. | 10 |
| Figure 1.8. Chemical structure of anionic lipid POPS (1-palmitoyl-2-oleoyl-sn-glycero-3-phospho-L-serine). | 15 |
| Figure 1.9. Chemical structure of zwitterionic lipid POPC (1-palmitoyl-2-oleoyl-glycero-3-phosphocholine), considered one of the model lipids for biophysical experiments. | 15 |
| Figure 3.1. SDS-PAGE gels obtained in the first purification strategy for the Httex1-37Q protein. | 28 |
| Figure 3.2. SDS-PAGE gels obtained in the optimized purification strategy for the Httex1-37Q protein. ... | 29 |
| Figure 3.3. ThT fluorescence assays for monitoring the amyloid fibril formation of tag-free Httex1-37Q. ... | 31 |
| Figure 3.4. SDS-PAGE gels obtained for the purification of His6-SUMO-Httex1-43Q fusion protein. | 33 |
| Figure 3.5. ThT fluorescence assays for tag-free Httex1-43Q in solution. | 34 |
| Figure 3.6. ThT fluorescence assays for Httex1-43Q. | 35 |
| Figure 3.7. ThT fluorescence assays for 5 μ M Httex1-43Q with anionic lipid vesicles. | 37 |
| Figure 3.8. ThT fluorescence assays for 10 μ M Httex1-43Q with anionic lipid vesicles. | 39 |

List of Abbreviations

| | |
|--|---|
| Aβ – Amyloid- β | NES – Nuclear exportation Signal |
| AFM – Atomic Force Microscopy | NLS – Nuclear Localization Signal |
| CNS – Central Nervous System | Nt17 – Domain with first 17 aminoacids |
| dNTPs – Deoxynucleotide triphosphates | O/N – Overnight |
| DTT – dithiothreitol | OD640 – Optical density at 640 nm |
| GST – Glutathione S-Transferase | PCR – Polymerase Chain Reaction |
| HD – Huntington's Disease | PMSF – Phenylmethylsulfonyl fluoride c |
| His₆ – tag with 6 histidines | polyA – domain with polyadenine |
| HTT – Huntingtin gene | polyQ – domain with polyglutamine |
| Htt – Huntingtin protein | POPC – 1-palmitoyl-2-oleoyl-glycero-3-phosphocholine1 |
| Httex1 - Huntingtin exon 1 | POPS –palmitoyl-2-oleoyl-sn-glycero-3-phospho-L-serine |
| Httex1-37Q – Huntingtin exon 1 with 37 glutamine residues | PRD – Proline Rich Domain |
| Httex1-43Q - Huntingtin exon 1 with 43 glutamine residues | PrP – Prion Protein |
| IAPP – Islet amyloid polypeptide | PTMs – Post Translational Modifications |
| IMAC – Ion Metal Affinity Chromatography | SCA1 – Spino-cerebellar ataxia 1 |
| IPTG – Isopropyl β -D-1-thiogalactopyranoside | SEC – Size exclusion chromatography |
| kDa – Kilo Dalton | SUMO – Small ubiquitin related modifier |
| Km - Kanamycin | T2D – Type II Diabetes |
| LUVs – Large unilamellar vesicles | TBLE – Total Brain Lipid Extract |
| MBP – Maltose Binding Protein | TEM – Transmisison Electron Microscopy |
| LB – Luria-Bertani, Miller's LB Broth | ThT – Thioflavin-T |
| MRI – Magnetic Resonance imaging | ULP1 – ubiquitin-like protein-specific protease 1 |
| MW – Molecular Weight | |

CHAPTER 1

INTRODUCTION

1.1 Neurodegenerative diseases and protein aggregation

In healthy organisms, proteins fold into their unique three-dimensional structure, known as their native conformation, and then perform their biological function. However, several neurodegenerative diseases are characterized by the formation of protein aggregates in the brain, causing harm to different brain regions and cell types, culminating in cell death. These aggregates are formed by proteins that cannot fold correctly or that cannot keep their native form for long [1].

There are several neurodegenerative diseases that are associated with protein misfolding and aggregation, namely the formation of amyloid fibers. Amyloid fibers are characterized by aggregation of proteins that form cross β -sheet conformation [2]. Cross β -sheets are formed by β -strands that assemble into ribbon-like structures, forming protofilaments. These protofilaments then assemble to form the amyloid fibrils. Among them, we have Alzheimer's Disease, Parkinson's Disease, Huntington's Disease and Type II diabetes. Huntington's Disease specifically is caused by a mutation in the huntingtin gene that leads to an expansion in the glutamine tract (polyQ) found in the first exon.

Table 1.1. A selection of human diseases where the formation of protein amyloid aggregates is an important feature and their respective pathological proteins. **Adapted from Chiti et al., 2017 [3].**

| Disease | Responsible protein | Structure |
|---|---|---------------------------------|
| Alzheimer's Disease | Amyloid- β peptide ($A\beta$) | Intrinsically disordered |
| Parkinson's Disease | α -Synuclein | Intrinsically disordered |
| Huntington's Disease | Huntingtin protein with expanded polyQ tract | Mainly Intrinsically disordered |
| Spino-cerebellar ataxia 1 (SCA1) | Ataxin-1 | Unknown |
| Type II Diabetes (T2D) | Islet amyloid polypeptide (IAPP) | Intrinsically disordered |
| Creutzfeldt-Jakob disease | Prion protein (PrP) | Intrinsically disordered |
| Pick disease | Microtubule-associated protein tau (τ) | Intrinsically disordered |

There are three main different approaches for studying amyloid fibrils: isolation of proteins from the brains of diseases patients, cloning and recombinant expression, or using synthetic methods to create synthetic peptides knowing the amino acid sequence of the pathological proteins [4]–[7].

Post translational modifications (PTMs) have been shown to influence the aggregation process of proteins involved in neurodegenerative diseases [8]. Through comparisons between healthy and diseases samples, it is possible to identify what changes are relevant for aggregation processes.

1.2 Formation of amyloid fibers and detection methods

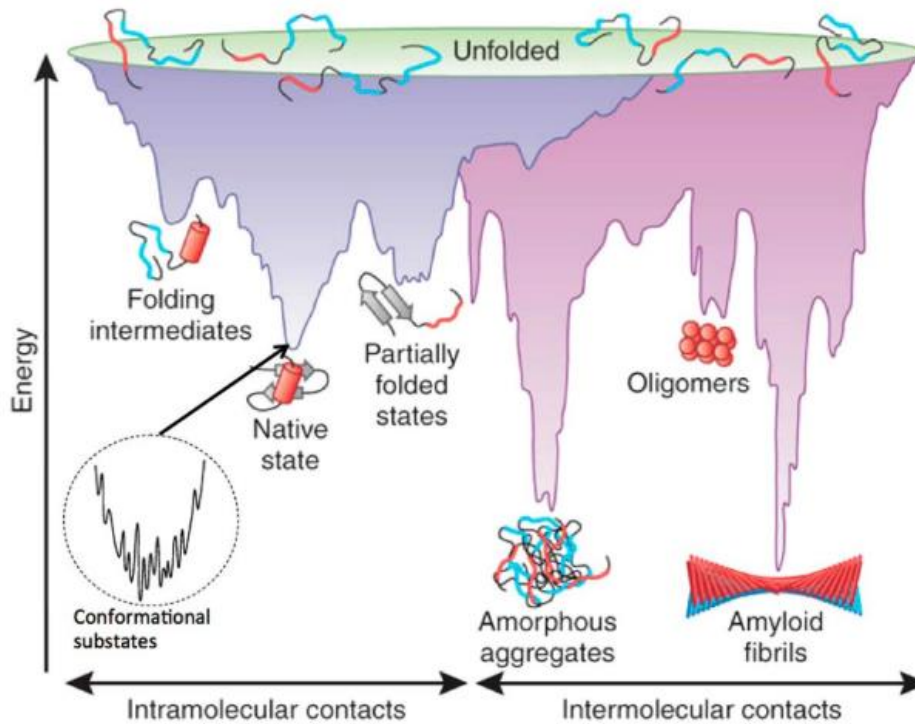


Figure 1.1: Schematic representation of the energy landscape for protein folding and aggregation. The landscape includes the free energy in relation to possible intra- and intermolecular contacts. Unfolded entities have the highest free energies and give rise to more stable structures with lower free energies; such states include the native state, as well as other lower energy states that are even more stable and harder to break, such as amyloid fibrils. **Adapted from Raskatov et al., 2017** [9].

The basic biological paradigm states that proteins show a structure-function relationship, where the structure of a protein will dictate its function. Proteins have a native structure, the conformation at which they can perform their biological function as intended [10]. It begins with the amino acid sequence that undergoes a series of conformational changes, usually mediated by chaperones [11]. However, mutations and other conditions inside the cell can cause this folding process to not function properly and the protein acquires other harmful conformations. Such is the case for many amyloid proteins, where other lower energy conformations are adopted, and the protein is unable to go back to its native structure [3]. Figure 1.1 illustrates the variety of protein conformations and their relative free energy.

The most widely accepted model for formation of amyloid fibrils is the nucleation polymerization model [12], [13]. The process begins with a lag phase where no aggregation is observed, but the formation of the nucleus begins. The nucleus is the highest energy unit in the fibrilization pathway, so makes the initial association process of the monomers entropically unfavorable [12]. Nucleation is thus a very slow and

rate-dependent process. In this stage, most of the environment contains the monomeric unit, the malformed peptide. The nucleation step involves the condensation of multiple molecular units and their association to form a protofilament. Once a critical nucleus is formed, the aggregation process accelerates exponentially, and other monomeric units connect to the structure to form the filament. Finally, filaments connect to form fibrils. The lag phase can be eliminated entirely if the sample already contains nucleated structures, commonly known as “seeds”.

The overall process is represented by a sigmoidal curve (Figure 1.2-A) involving three main steps: lag phase where nucleation happens, growth phase where elongation happens, and saturation phase where the protofilaments bind to form amyloid fibers. Figure 1.2-B explains the three main steps in amyloid fiber formation.

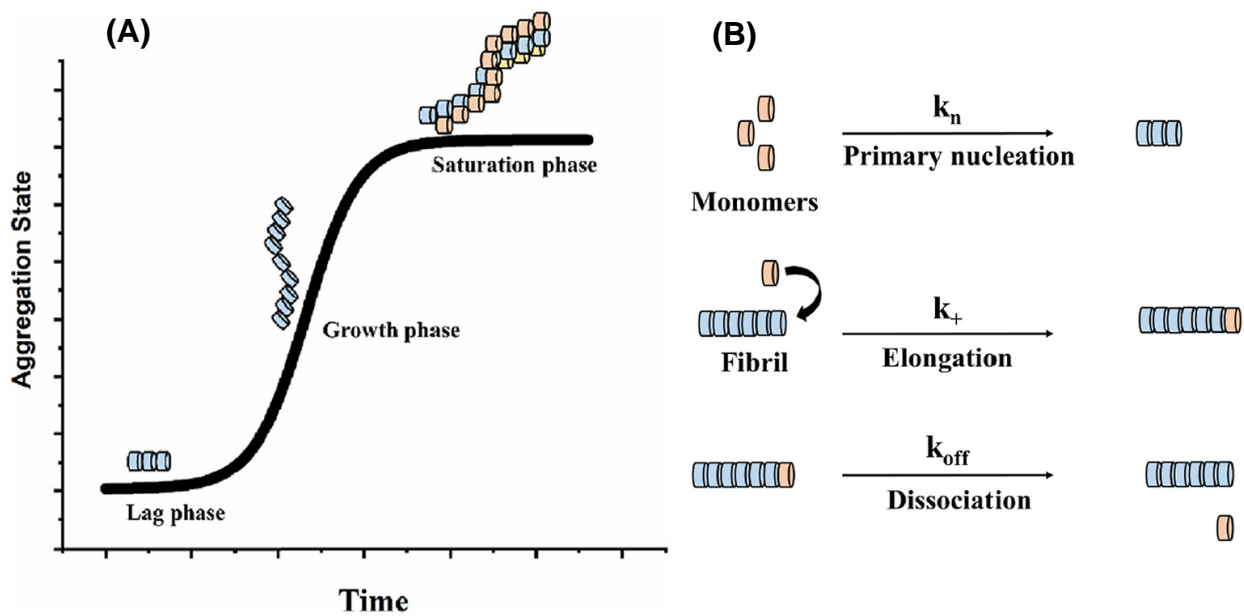


Figure 1.2: (A) General aggregation profile of proteins that follow a nucleation-polymerization pathway for amyloid fiber formation. (B) Representation of the process of nucleation, elongation, and dissociation in the process of amyloid fibril formation. **Adapted from Sharma et al. 2021 [12].**

Knowing that amyloid fibrils play a major role in the pathogenicity of several neurodegenerative diseases, studying their atomic structure can aid in understanding their formation process. Dyes and fluorescent markers are often used to detect amyloid fibrils.

There are several ways to detect the presence of amyloid fibrils, using both probes and microscopy techniques. One of them is cryogenic electron microscopy (Cryo-EM), a technique that gives a high-resolution representation of the structure of amyloid fibrils [14]. Another technique is fluorescence-lifetime imaging microscopy (FLIM), which allows detection of the fast and very sensitive amyloid aggregation

process [15]. FLIM relies on the measurement of exponential fluorescence decays over time and spatial resolved images and kinetic aggregation information can be obtained. Another method is structured illumination microscopy (SIM), where the fluorescence excitation light is scattered and it generates a patterned illumination that can be rearranged to obtain the necessary data [15]. It has been used to monitor fibril formation in live-cell imaging experiments with fine structural details of the samples [16]. More structural data can be obtained by imaging techniques such as TEM (Transmission Electron Microscopy), or AFM (Atomic Force Microscopy) [17], [18].

Congo Red birefringence assay is a traditional histological technique used to identify the presence of amyloid deposits *in situ*, *ex vivo*, and *in vitro* [13]. The dye shows yellow-green birefringence under polarized light, that is, stained samples appear red at normal light but yellow-green between crossed polarizers. It is the first step for the generic identification of proteins forming amyloid structures, since this dye has affinity for binding to fibril proteins containing β -sheet conformation, the hallmark of amyloidogenic proteins [19].

Thioflavin-T (ThT) fluorescence assays measure the change in fluorescence intensity of ThT after it binds to amyloid fibrils [13], [20]. In this thesis, ThT fluorescence spectroscopy assay was the method used to identify and follow the amyloid formation and protein aggregation process over time. ThT is one of the most common techniques used to identify the presence of amyloid fibrils in samples. After it binds to the amyloid fibrils, ThT gives a strong fluorescent signal at approximately 482 nm, when excited at 450 nm [21].

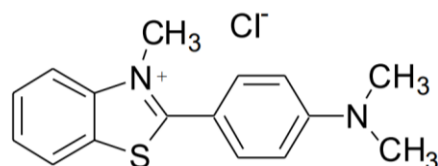


Figure 1.3: Chemical structure of Thioflavin-T (ThT) dye used for identification of amyloid structures. Adapted from Khurana et al. 2005 [22].

ThT acts as a “molecular rotor”: when in solution, the rings in the chemical structure (Figure 1.3) rotate freely. The increase in fluorescence happens when ThT binds to amyloid fibrils and causes the rotational immobilization of the central C–C bond connecting the two rings in the structure. An advantage of ThT when compared to Congo Red (CR) is its simplicity in usage – unlike CR, ThT does not need staining and washing steps and can be applied directly to the sample [23]. However, care is needed because false positives can be obtained when working with CR. ThT has also been shown to bind and emit fluorescence when bound to fibers prepared from biological or synthetic sources. All of this makes ThT a very sensitive and efficient tool.

ThT has been successfully used to study amyloid proteins with varied amino acid sequences, thus strongly suggesting that it recognizes a structural feature common among fibrils, rather than a specific sequence. Knowing that amyloid fibrils in general show a cross- β organization, it is generally well accepted that the ThT binding site is located on the surfaces of cross- β structures, a hallmark of amyloid proteins.

Figure 1.4 shows a schematic representation of amyloid fibrils with their anti-parallel organization. A cross β -strands, there are repeating interactions of side chains that form extended channel-like motifs. This arrangement generates space that is exposed to the solvent and allows the binding of linear dyes to the side chains along the axis of the fiber, such as ThT or Congo Red [21], [23], [24]. Of course, there are other proposed models for ThT binding, but the “channel model” is the most accepted.

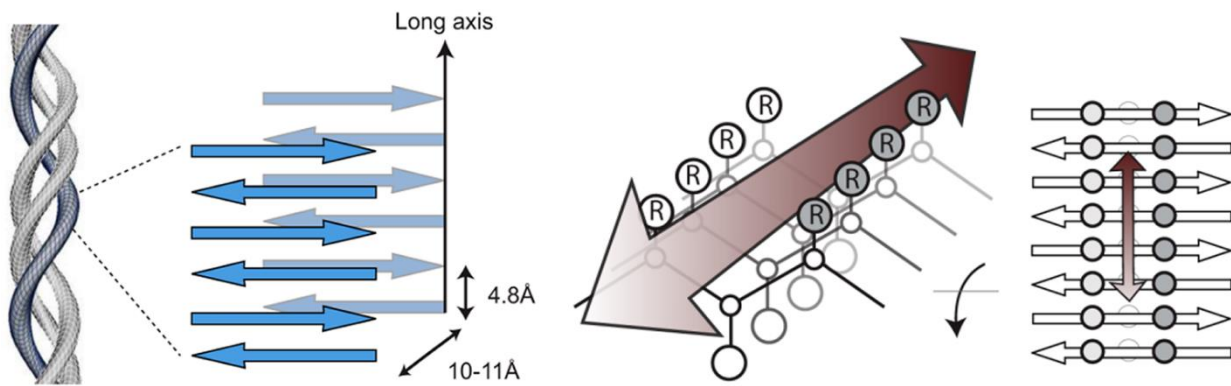


Figure 1.4: (A) Schematic representation of cross- β amyloid structures and distances between components, in Angstrom. (B) Schematic representation of the proposed model of ThT binding to amyloid fibrils via interaction with the side chains exposed to the solvent. It is proposed that the minimal span required for ThT binding is four consecutive β -strands. **Adapted from Biancalana et al. 2010 [23].**

Research done by Xue et al. 2017 [25] show that ThT fluorescence intensity correlates linearly with amyloid fibril concentration, even when different concentrations of both dye and fibrils were tested. It was also shown that ThT has little or no effect on the aggregation kinetics. Therefore, ThT has been extensively used for monitoring amyloid fibril formation.

The combination of different detection methods helps understand the process of fibril formation both in a general and detailed manner. However, interpreting results of aggregation should be performed carefully, since aggregation samples are heterogenous, containing oligomers, fibrils and inclusion bodies that might generate differences in emitted and recorded signals.

1.3 Huntington's Disease (HD)

Huntington's Disease (HD) is a fatal autosomal dominant neurodegenerative disease caused by a CAG trinucleotide repeat expansion within the first exon (Exon 1) of the huntingtin gene (*HTT*, *IT15*) located on chromosome 4 [26]. Pathological CAG expansions lead to the expression of a mutant huntingtin protein (Htt) containing an expanded polyglutamine (polyQ) domain, which alters its physicochemical properties and cellular stability [27]. HD presents a progressive nature. Several studies also report a strong correlation between the polyQ-length and the age of onset in HD, symptoms appear earlier for longer polyQ-lengths [28].

The wild-type *HTT* gene is composed of 11 to 34 CAG repeats. Abnormal CAG expansions greater than 40 represent a near-certain possibility to develop HD, whereas CAG repeats between 34 and 40 show medium penetrance, with no disease or a very late age of onset. Zühlke et al. has reported the propensity of CAG repeats to expand through generations due to meiotic instability [29].

The most famous case study of HD happened in Lake Maracaibo in Venezuela, where several families have been developing HD [30]. Researchers have monitored these families to collect clinical and genetic data for further studies. Patients are descendants of a woman who passed the abnormal mutated gene responsible for HD.

HD has been studied through several methods, from post-mortem tissue analysis to usage of transgenic murine animal models [31] and several cell lines, including *in vitro* assays with isolated proteins and synthetic peptides that mimic the toxic Htt protein. *In vivo* magnetic resonance imaging (MRI) has shown that HD impacts brain morphology, causing loss in volume of grey and white matter, micro- and macrostructural changes, as well as changes in functional brain activity [5].

1.4 Symptoms, diagnosis and treatment

HD impacts both the physical and psychological wellbeing of the patients. The disease typically begins showing its symptoms in mid-life, but there is variety at the exact age of onset which has been attributed primarily to variation in the CAG length [32], [33].

Physical symptoms include chorea (involuntary and irregular muscle movements) and balance disturbances. Chorea is the most recognizable and treatable symptom in HD. Unfortunately, the decline in motor control and postural instability lead to falls and places the patient at risk of serious injuries [34]. Psychological and psychiatric symptoms include many emotional distress signals, such as depression, anxiety and suicidal ideation [35], [36]. Patients also show a decrease in cognitive abilities: speed of processing, problem-solving, and attention [37], [38]. It is possible to detect the onset of cognitive impairment before motor manifestations appear, but ultimately the rate of cognitive decline increases as patients near the motor onset.

The most direct and effective tool for diagnosis of HD is genetic tests that measure the CAG length in the *HTT* gene [39]. However, this method is not accurate in indicating the age onset for the symptoms. The

diagnosis process is also accompanied by screening for motor symptoms that unequivocally point towards HD, along with confirmed family history of the disease or a positive genetic test [40]. Prenatal testing is also a tool for HD patients that are concerned about passing the disease to a child.

Unfortunately, there is no current cure or disease-targeting treatment available. Most care is directed towards managing physical and psychological symptoms, as it is not possible to slow neurodegeneration [41]. Future research is focused on genetic engineering, aiming to remove the CAG repeats in the patient's DNA or RNA. Possible strategies for this include CRISPR/Cas-9 (DNA) and antisense oligonucleotides (RNA) [42], [43].

1.5 Huntingtin protein (Htt)

Htt protein is encoded by the *HTT* gene located on chromosome 4 in humans. The protein is expressed in all tissues of the body, but research focuses on its role in the degradation of the central nervous system (CNS) [44]. The pathological region of the mutant gene corresponds to exon 1 out of a total of 67 exons. Exon 1 has been extensively studied due to its established role in HD. The polyQ tract is flanked by a 17-amino acid segment at N-terminal and a C-terminal proline-rich domain (PRD) [45]. The full-length Htt protein contains 3144 amino acids and has a molecular weight of 348 kDa [46]. Several studies have identified a myriad of post-translational modifications (PTMs) at numerous amino acids, including phosphorylation, acetylation, ubiquitination, sumoylation, among others [47].

The overall Htt structure includes units of around 50 amino acids that repeat themselves throughout the protein, creating HEAT repeats. These repeats are composed of two anti-parallel alpha-helices with a helical hairpin configuration [48], [49]. Figure 1.5 summarizes many of the Htt protein's characteristics.

The exact function of the Htt protein remains unknown, but evidence supports its role in cell division, transcriptional regulation, and intracellular transport [46]. Previous research pointed out its importance in normal embryogenesis, as knockout mice for the *HTT* gene die at early developmental stages [51]. Moreover, Htt protein also comprises several signal sequences - nuclear export signals (NES) and nuclear localization signals (NLS), suggesting that its location alternates between the cytoplasm and nucleus as required [44].

Htt plays an important role in vesicle trafficking in neurons since its phosphorylation has been reported to act as a switch between retrograde and anterograde transport [52]. It is suggested that Htt associates with vesicles and microtubules by binding to dynein (a microtubule motor protein), and HAP1 (Huntingtin Associated Protein 1), highlighting Htt's role as a scaffold and its importance in protein-protein interactions. The study proposes a model where Htt has a key role in promoting association of vesicles with the cytoskeleton by directly binding to dynein and thus affecting cytoplasmic vesicle motility [53]. The Htt protein also contains polyQ and polyP sequences that form polar zipper structures that are able to interact with DNA, likely to regulate gene transcription as it also interacts with known transcription factors and repressors [44].

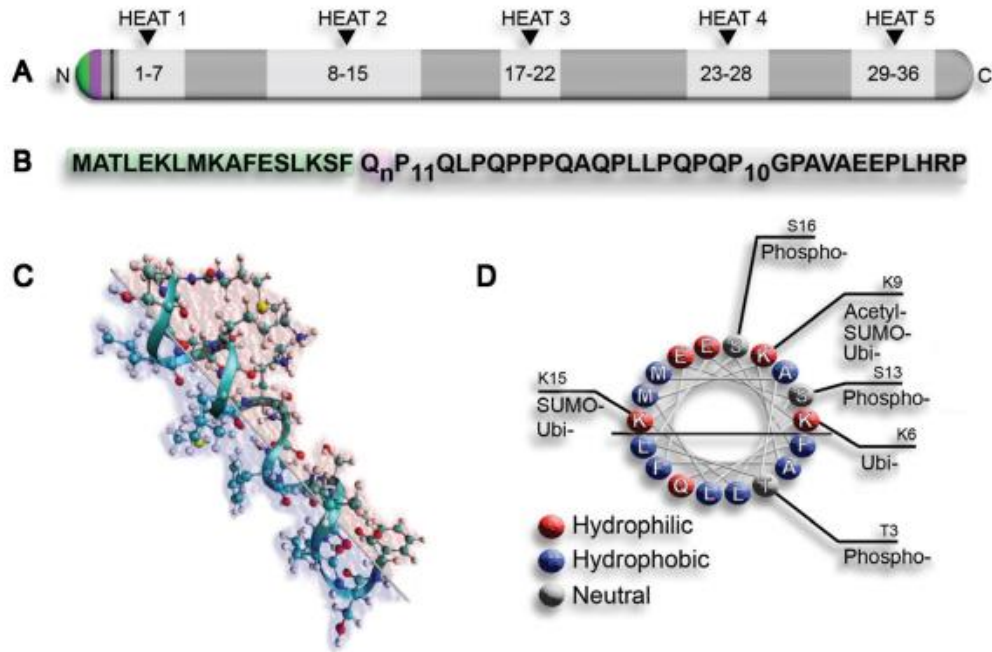


Figure 1.5: Schematic representation of several features of Htt. (A) Full length Htt protein with HEAT repeats. The black stripe represents the end of Httex1. (B) Sequence of Httex1 and its domains: the first 17 amino acids (Nt17) are shown in green, polyQ in purple, proline rich domain (PRD) in gray. (C) Theoretical three-dimensional structure of Nt17 forming a α -helix. The hydrophilic region is shown in red while the hydrophobic region is shown in blue. (D) View down from the barrel of the α -helix showing the relative hydrophobicity level, as well as the sites known to be a target for PTMs. **Adapted from Arndt et al., 2015 [50].**

As mutant huntingtin keeps being produced, if it does not aggregate to form amyloid fibers, the free, diffused form will interfere with proteasome stability by occupying molecules responsible for protein folding and interfere with the normal interactions found in the proteasome [54]. Mutant huntingtin was also found to disrupt transcription.

1.6 Huntingtin exon 1 (Httex1)

About a decade ago, Sathasivam et al. [55] found that the formation of the small and toxic fragment at the N-terminal is caused not only by the proteolytic cleavage as proposed previously, but by also aberrant splicing of the translated mRNA with the involvement of a splicing factor (figure 1.6) [55].

A study done by Graham et al. [56] was able to identify critical cleavage sites by caspase-6 (protease) in mutant huntingtin involved in the generation of toxic fragments that play a role in the neuro-pathogenesis of HD. This conclusion was taken when inhibition of caspase-6 was observed to protect against striatal volume and neuronal loss.

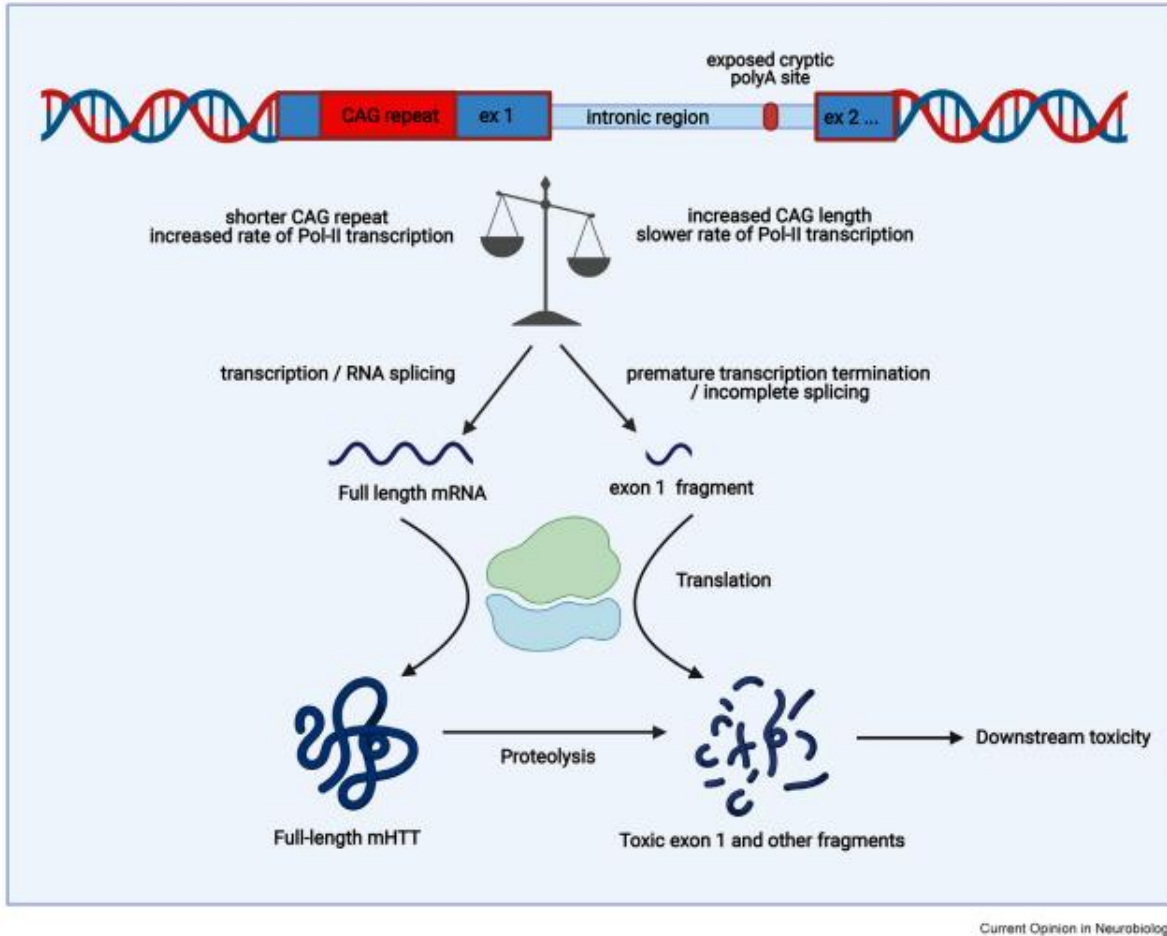


Figure 1.6: The proposed mechanism for the incomplete splicing and proteolysis. Longer CAG repeats cause reduced rates of transcription by polymerase II, which leads to incomplete splicing. This slower rate may give more time for transcription factors to identify exposed cryptic poly-adenylation (polyA) sites, and consequently generate truncated toxic exon 1 fragments. Alternatively, the entire mRNA corresponding to the full-length HTT protein can be translated and via proteolysis generates the toxic exon 1 fragment responsible for most of HD's pathology. **Adapted from Bunting et al. 2022** [56].

In HD patients, the Httex1 sequence includes the extended polyQ section, flanked by the N-terminal domain containing the first 17 amino acids (Nt17 domain) and the C-terminal proline rich domain (PRD). Some studies have highlighted the role of the flanking polyQ domains in the aggregation phenomenon [57], [58], [59]. The aggregation phenomenon follows a nucleated growth polymerization pattern [57]. First, there is the energetically unfavorable formation of a nucleus, followed by the growth of the aggregates by sequential monomer addition. The same study highlights the contradictory effects that Nt17 and PRD seem to have on the aggregation of the fragments: the PRD sequence located on the C-terminal side of

the polyQ does not change the aggregation mechanism at its core, but it reduces the aggregation kinetics and aggregate stability [58].

On the other hand, the Nt17 domain seems to act as a catalyst to the aggregation process. A study [57] used a synthetic peptide sequence of the Nt17 domain of the HTT gene attached to 35 glutamine residues to prove this. When equal concentrations of the Nt17-polyQ35 and the polyQ35 were compared, the results showed that the sequence containing the Nt17 domain aggregates significantly faster. The same study was able to show this effect is dominant over the aggregation-suppressive effect the PRD. Nt17 domain plays an important role in aggregation as a first step in the process – this is further supported by an experiment where binding of immunoglobulin fragment to N-terminal domain is shown to inhibit Httex1 aggregation and toxicity in a variety of cell models [60]. Just as longer polyQ segments *in vivo* are associated to earlier age of disease onset, the length of artificial polyQ peptides greatly influence the aggregation kinetics.

Figure 1.7 shows a schematic representation of the possible aggregation pathways for the Htt protein. The aggregation process starts with a lag phase up until a certain threshold, after which a rapid elongation phase is observed, marked by aggregate growth. Curiously, the study was able to show that the lag phase can be drastically reduced, if a small amount of already aggregated polyQ peptides is added.

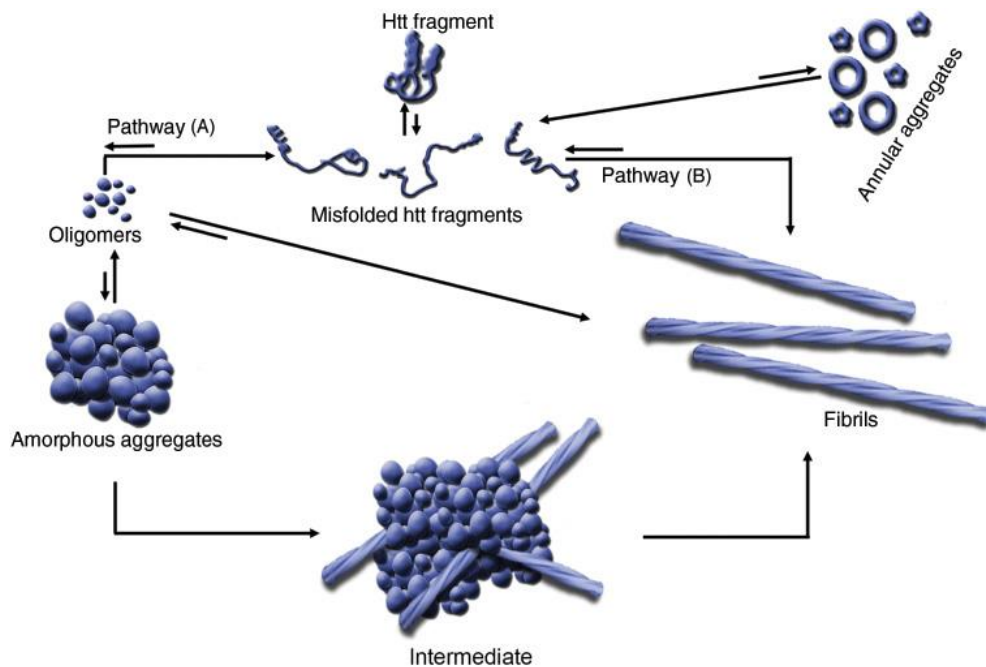


Figure 1.7: The proposed model for polyQ aggregate nucleation and extension. The Htt fragment once produced can adopt several misfolded conformations, such as oligomers or annular aggregates. The figure shows two possible pathways for fibril formation: A and B. In pathway A, there is the formation of

oligomer intermediaries, which then form amorphous aggregates among themselves. These aggregates can also accumulate together and form large inclusion bodies, a known hallmark of HD. A major structural transformation must occur within the aggregates to initiate the fibril formation process. Pathway B describes the direct transition from monomeric units to fibrils. **Adapted from Arndt et al., 2015 [50].**

1.7 Recombinant Expression and purification of Httex1

Due to the high content of glutamine and proline amino acid residues in Httex1, both charge-neutral amino acids, the fragment is unstable and prone to aggregation, thus complicating the purification strategies. This means that traditional systems, like recombinant bacterial and mammalian expression, become even more challenging and unfeasible without extra steps [61].

For this reason, initial Httex1 studies used synthetic polyQ [62] or Httex1-like peptides containing additional features (such as addition of lysine amino acids or other charged amino acids) that make solubilization of the protein easier, especially for Httex1 fragments with a large polyQ-length, which are notably much harder to isolate and purify [57, p. 1]. However, these methods may not give sufficiently accurate or extrapolative data regarding the Httex1 protein that is expressed in HD patients. The method still poses its advantages: the usage of artificial peptides eliminates the troubles posed by the presence of impurities that could interact with the aggregate-formation process.

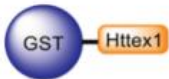













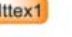















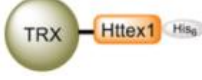


Another strategy adopted by researchers is the fusion of Httex1 fragment to large solubilizing protein tags, such as glutathione S-transferase (GST), maltose binding protein (MBP), or thioredoxin [61]. This technique requires proteases to cleave the fusion protein *in situ* – due to Httex1's nature, the release of the fusion protein will initiate the aggregation of the fragments.

A possible issue with fusion technique is the incorporation of additional amino acids at the N- or C-terminal of the protein, which in turn can alter the biophysical and biochemical properties. Not only that, but certain proteases may cleave regions within the Nt17 domain, resulting in the formation of undesired Httex1 fragments.

If any of these issues occur, the result will be a heterogeneous mixture of variations of the desired fragment. This also requires enzymes that perform a complete cleavage, as well as high specificity and efficiency to minimize the insertion of unwanted characteristics as much as possible.

Additionally, the fusion proteins mentioned in the beginning of this section are large when compared to the Httex1 fragment, thus rendering small conformation changes, such as modifications in secondary structure, more difficult to observe.

Table 1.2: Table containing a list of the most common Httex1 fusion proteins and proteases used for *in vitro* aggregation studies. **Adapted from Vieweg et al. 2016 [63].**

| Httex1 fusion protein | protease | remaining sequence post-cleavage | comments |
|---|----------------------|---|--|
|  | Trypsin |  | trypsin cleavage behind Lys ₆ , Lys ₉ , Lys ₁₅ and Arg ₈₉ create truncated Httex1 fragments ^a |
| | Trypsin Factor Xa |  Gly-Ile-Arg-  | trypsin cleavage behind Lys ₆ , Lys ₉ , Lys ₁₅ and Arg ₈₉ create truncated Httex1 fragments ^a |
| | PreScission | Gly-Pro-  | |
|  | TEV | Gly-  -S-tag | |
|  | PreScission | Gly-Pro-  | |
|  | PreScission | Gly-Pro-X-  -  -Cys | X: unknown vector-derived residues |
|  | PreScission | Gly-Pro-  -  | |
|  | | Gly-Pro-  -  | |
|  | Thrombin | Gly-Ser-  -  | thrombin miscleavage between K ₁₅ and S ₁₆ creates a truncated Httex1 fragment ^b |
|  | Thrombin | Gly-Ser-  -  -  | thrombin miscleavage between K ₁₅ and S ₁₆ creates a truncated Httex1 fragment ^b |
|  | Factor Xa |  -  | |
| | TEV | Gly-Ala-  -  | |
|  | EKMax |  -  | |

In 2018, Reif et al. [63] published an optimized protocol where tag-free Httex1 is generated in milligram quantities; this technique relies on the transient fusion of small ubiquitin related modifier (SUMO) which will be cleaved by ubiquitin-like protein-specific protease 1 (ULP1). The advantage of using ULP1 is that it does not recognize a specific sequence, but rather it recognizes the tertiary structure of the SUMO protein – this eliminates the problems caused by miscleaving of the sequence, which as mentioned before could

add or remove amino acids to the Httex1 fragment. Another advantage of using ULP1 is its fast-cleaving time. Previous strategies, such as the intein process, required some hours for complete cleavage to occur, thus allowing the formation of aggregates to begin before complete cleavage was observed. Yet another advantage of this method is its absence of an external protease for it to function because cleavage of intein tag occurs by change in pH [64]. This possibly avoids the possibility of premature cleaving that has been observed in previous methods.

A polyhistidine (His₆) tag was also present in the construct to facilitate the purification of the protein via Immobilized Metal Ion Affinity Chromatography (IMAC) – thus the final construct to be expressed is the Httex1 fragment with the His₆-SUMO tag at the N-terminal region.

The Httex1 fragment is intrinsically disordered, thus being especially prone to degradation: the presented protocol does not pose any threat of Nt17 domain degradation, however truncations in the PRD domain remain a possibility. This is quite worrying as the resulting truncated proteins retain many of the original fragments' properties, such as hydrophobicity, charge, and size, and thus removing them from the obtained sample after the cleaving of the His₆-SUMO is very challenging. Luckily, the protocol suggests that always working on ice and using sufficient protease inhibitor should keep the PRD degradation levels low [63]. Due to its very high propensity to form aggregates, the cleaved fragment should be prepared for purification as soon as the cleaving reaction is over.

In the event that aggregation occurs, a disaggregation and resolubilization protocol is also included in the article published by Reif at al. [63] to avoid obtaining misleading data from the kinetic and physical studies. Such misleading data could arise from the presence of pre-formed aggregates in the sample after it has been cleaved and stored, so it is important to perform this step to guarantee that most of the sample is composed of monomeric units.

The use of the SUMO tag, which provides the SUMO-Httex1 construct with high solubility and stability, allows researchers to further manipulate the Httex1 before cleaving and even before expressing by introducing alterations at cNDA – this approach would allow for the introduction of post-translational modifications, addition of fluorophores and other markers and labels, in turn proving as additional tools to help us understand the structure-function relationships as well as pathological strategies contained within the Httex1 fragment.

1.8 Kinetics and lipids

The formation of amyloid fibrils is the hallmark of several neurodegenerative diseases, so understanding the mechanisms and kinetics of their formation is paramount. The standard protocol for investigating fibril formation is the ThT fluorescence assay, where ThT binds to the β -sheet structure present in amyloid fibrils and emits intense fluorescence when compared to free ThT levels in solution. However, this technique also poses several difficulties. Results can sometimes be ambiguous due to differences in pH, temperature, selected buffers, preparation of the protein samples, and additives or impurities present in

the solution [20]. The obtained kinetic data should present a curve whose profile is similar to the sigmoidal curve shown in Figure 1.2-A.

Lipid membranes

Lipids are an important part of every cell, as every cell is encapsulated by a lipid bilayer and human cells have several sub-cellular compartments (organelles) that are also encapsulated by lipids, such as the endoplasmic reticulum, mitochondria, and the Golgi apparatus [65], [66]. Amyloid fibrils interact with lipid surfaces, disrupting the cellular stasis. Studying this interaction is fundamental work and has potential implications for disease understanding [67].

The kinetic assays including lipid membranes make use of either biological or synthetic lipids. Biological lipids include total brain lipid extract (TBLE) and synthetic lipids use negative or zwitterionic lipids, or a mixture of both.

TBLE is usually chosen as a model lipid system for surface interaction studies because it is composed of several lipids in a ratio like that of a biological system [68]. It is more complex than synthetic membranes; besides containing phospholipids, it also contains cholesterol, sphingolipids, and other components [69].

The Nt17 domain has been proven to form an α -helical structure and act as a lipid binding domain that interacts with membrane curvature and is subjected to electrostatic interactions with headgroup charges [70]. This makes the Nt17 domain an extremely important feature that facilitates the insertion of the amyloid fibrils into the lipid membranes [71]. Because of this, it has a negative role in membrane stability, affecting the bilayer's fluidity by increasing its rigidity [18].

Several results support the notion that htt fibrils bind to the membrane and membranes of subcellular components, affecting the membrane's integrity and stability. Not only that, but the anchoring of fibrils and aggregates at the lipid membrane can serve as a "seed" for the monomers to aggregate and exponentially increase the fibrillation rate and creating areas on the cellular surface where the concentration of mutant htt is very high.

On the other hand, the PRD rich domain has been shown to be less important when it comes to lipid interaction and the insertion of the protein in the lipid membrane. Results from literature show that the presence of the PRD alone is not sufficient for insertion into the lipid membrane, but that it had a considerable effect on aggregation and formation of aggregates when the Nt17 domain is also present in the protein or construct [71].

To form a lipid membrane, this thesis uses a mixture of negative and zwitterionic lipids on a ratio of 25% POPC and 75% POPS. The zwitterionic lipid is overall charge neutral and it has been included in the mixture to equilibrate the overall charge of the lipid membrane, as using only anionic lipids could cause repelling between the headgroups. This simplification of a biological lipid membrane allows researchers to study the fundamental mechanisms through which fibrillation of httex1 can be effected [17]. In future

studies, other components can be gradually added to this mixture to test their influence and interaction in the fibrillation process.

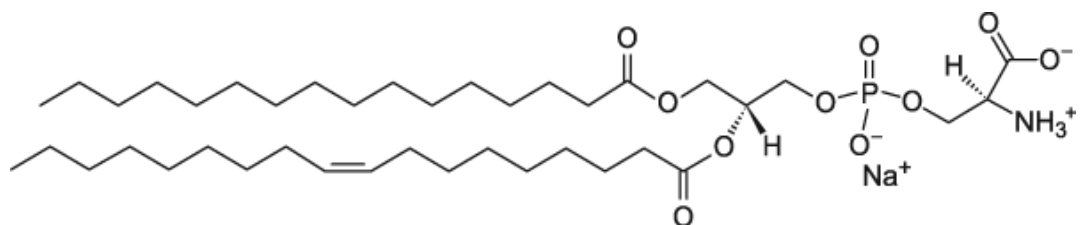


Figure 1.8: Chemical structure of anionic lipid POPS (1-palmitoyl-2-oleoyl-sn-glycero-3-phospho-L-serine).

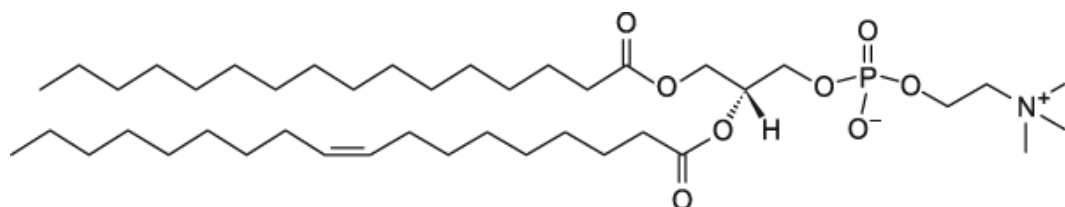


Figure 1.9: Chemical structure of zwitterionic lipid POPC (1-palmitoyl-2-oleoyl-glycero-3-phosphocholine), considered one of the model lipids for biophysical experiments.

Goals and work-plan

It has been suggested in literature that lipidic membranes have an enormous effect on the fibrillation of amyloid proteins. This has been speculated to happen due to electrostatic interactions between the negative charges present in lipid membranes and the flanking domains of amyloidogenic proteins, in this particular case, the mutant huntingtin protein.

The overall goal of this work is to assess how the presence of anionic lipidic membranes affects the kinetics of the fibrillation process of mutant Htt via ThT fluorescence assay. For this, lipid membranes consisting of 75% anionic lipid POPS and 25% zwitterionic lipid POPC were prepared. The addition of the zwitterionic lipid was done to stabilize the membrane by preventing negative repelling. It is expected that the presence of the lipid membrane will increase the aggregation rate of mutant Htt.

The following steps were necessary to obtain the results of this thesis:

- First, *E. coli* cells were transformed with the vector containing the mutant Htt protein with the SUMO and His₆ tag. The cells were grown and induced with IPTG to express the fusion protein of interest that will be further purified through IMAC and SEC procedures. Finally, the concentration of the obtained purified fractions is determined, and the fractions of interest are stored at -80 °C.
- Next, the lipid vesicles containing POPS and POPC need to be prepared. The end goal is to obtain LUVs via extrusion. The LUVs are then stored in the buffer that will be used for the kinetic assays with ThT. This implies that LUVs will be stored in aqueous buffer and thus will not remain stable for long periods of time. The LUVs should be used in the kinetics assays planned throughout the following days.
- Finally, the Tht fluorescence assay will allow the detection of amyloid fibrils. The fluorescence assay with microplates will measure the fluorescence over a period of 16 hours. That will also allow the tracking of the formation of amyloid fibers, from the lag phase until a plateau is reached.

CHAPTER 2

MATERIALS AND

METHODS

2.1 Plasmids, bacterial strains, materials and chemicals

Both pET-SUMO-Httex1-37Q/43Q plasmids were previously created in the host lab. The Httex1-37Q or -43Q cDNA were obtained by polymerase chain reaction (PCR) from the pTWIN1-His₆-Ssp-Httex1-37Q/43Q plasmids (gift from Hilal Lashuel - Addgene plasmids #84351 and #84352, respectively) and further subcloned into a pET SUMO vector obtained from Invitrogen. The pET-SUMO-Httex1-37Q/43Q plasmids allow to express Httex1-37Q/43Q fused at N-terminal with a tag containing a polyhistidine (His₆) and a small ubiquitin-related modifier (SUMO) [61]. *E. coli* chemically competent One Shot® Mach1™-T1^R and BL21(DE3) were also obtained through the Champion™ pET SUMO Protein Expression System (Invitrogen). Deoxyribonucleotide triphosphate (dNTPs) Mix and FastDigest DpnI are from Thermo Fisher. PfuUltra High-fidelity DNA Polymerase is from Agilent Technologies. Primers for site-directed mutagenesis were synthesized by Stab Vida; DNA sequencing was also carried out by Stab Vida.

Luria Broth (Miller's LB Broth), agarose, isopropyl β-D-1-thiogalactopyranoside (IPTG), dithiothreitol (DTT), kanamycin (Km) and NZY Miniprep Kit for plasmid extraction/purification were obtained from NZYTech. The complete Mini EDTA-free Protease Inhibitor Cocktail Tablets are from Roche. Phenylmethylsulfonyl fluoride (PMSF) is from PanReac AppliChem. The 0.45 μm syringe filters (low protein binding) were obtained from Labbox. The Amicon Ultra-15 Centrifugal Filters with 3 kDa and 10 kDa cutoff were purchased from Millipore. Slide-A-Lyze™ Dialysis Cassettes of 10 kDa cutoff (30 mL) and the dialysis as well as the Pierce™ Modified Lowry Protein Assay Kit were obtained from Thermo Fisher. The 5 mL and 1mL HisTrap FF columns and also the Superdex 75 10/300 GL column are from GE Life Sciences.

POPC and POPS were purchased from Avanti Polar Lipids. ThT is from Sigma and the 96-well microplates F-bottom and non-binding protein are from Greiner Bio-One.

The chemicals used for preparing buffers and solutions for Httex1 production, SDS-PAGE gel, and the Httex1 aggregation assays were obtained from different providers (typically NZYTech, Sigma and Thermo Fisher). Buffer solutions were always made with Milli-Q water (18.2 MΩ.cm), filtered with 0.2 μm membrane filters (Sartorius), and finally stored at 4°C.

2.2 Site-directed mutagenesis of pET-SUMO-Httex1-37Q

For future Httex1-37Q-lipid interaction studies and to create single-labeled Httex1-37Q constructs at both flanking polyQ regions, the pET-SUMO-Httex1-37Q plasmid was engineered for expression of Httex1-37Q containing a single-cysteine mutant at position A2C or A82C. The mutations were introduced by QuikChange II Site-Directed Mutagenesis strategy (Agilent Technologies) according to the manufacturer's instructions. The pET-SUMO-Httex1-37Q plasmid previously cloned in the host Lab was used as a template. Briefly, we used the following PCR reaction mixtures: 5 μL of 10x PfuUltra HF reaction buffer, 1 μL of 40 mM of dNTPs mixes, 1.25 μL of 0.1mg/ml of each primer (for 125 ng), 30 ng of template, 1 μL of PfuUltra High-Fidelity DNA polymerase and then water for a final volume of 50 μL. The PCR was

performed in a SimpliAmp Thermal Cycler (Thermo Fisher) and using the following settings: (i) an initial denaturation at 90 °C for 30 seconds, and then (ii) 16 PCR cycles- 30 seconds at 90 °C for denaturation, 1 minute of annealing at 55 °C, and 12 minutes at 68 °C for extension. The plasmid amplification was confirmed in a 1% agarose gel (100 V for 50 min).

Table 2.1: Sequence of the primers used for site-directed mutagenesis.

| Primers | Sequence (5' to 3') |
|---------------------|--|
| A2C Forward | CAGAGAACAGATTGGTGGTTGTACCCTGGAAAACTGATG |
| A2C Reverse | CATCAGTTTTTCCAGGGTACAACCACCAATCTGTTCTCTG |
| A82C Forward | CCGGGTCCGGCAGTTTGTGAAGAACCGCTGCATC |
| A82C Reverse | GATGCAGCGGTTCTTCACAACTGCCGGACCCGG |

The PCR reaction was then incubated with 1 µL of FastDigest DpnI at 37°C for 1 hour. Afterwards, One Shot® Mach1™-T1^R Chemically Competent *E. coli* cells were transformed with 4 µL of the digested PCR product by heat shock method and spread on LB-Agar plates containing 50 µg/mL of Km. Single isolated colonies were inoculated in 30 mL of LB-Km medium and then left to grow overnight (O/N) at 37 °C with 200 rpm shaking. The plasmid extractions were performed with the NZYMiniprep kit according to the manufacturer's instructions. The concentration and purity of DNA were measured using the NanoDrop™ One/OneC spectrophotometer (Thermo Fisher). Samples were then sequenced by Stab Vida using a T7 reverse primer (5' TAGTTATTGCTCAGCGGTGG 3').

2.3. Production of tag-free Httex1-37Q

2.3.1 Expression test and large scale expression of His6-SUMO-Httex1-37Q

BL21(DE3) One Shot® chemically competent *E. coli* were initially transformed with the pET-SUMO-Httex1-37Q plasmid by heat shock, spread on a LB-Agar plate with Km and incubated O/N at 37 °C. A 25 mL LB-Km O/N inoculum of a single colony was then performed at 37°C with 200 rpm shaking. In the next morning, the culture was renewed by using 15 mL of the O/N culture and 100 mL of fresh LB/Km medium that was further incubated for nearly 4 hours under the same conditions.

For the expression test, 400 mL LB-Km medium was inoculated with the previous culture for an optical density at 640 nm (OD₆₄₀) of 0.1. The cells were left to grow at 37 °C and 250 rpm until reaching an OD₆₄₀ between 0.4 - 0.8. For evaluating the best IPTG concentration for protein expression, the 400 mL culture was then divided into four different culture flasks (each containing 100 mL) for exploring distinct IPTG concentrations (0.4, 0.6 and 0.8 mM were added) or auto-induction (without IPTG). The cells were further incubated O/N at 16°C with 250 rpm shaking.

Samples were taken before and after the IPTG induction for a volume calculated in equation (1) to keep the same OD across all samples.

$$V = \frac{1.2}{OD_{640}} \quad (1)$$

These samples were then centrifuged at 8000 rpm for 2 minutes at 4 °C and the pellet was resuspended in 80 µL of loading buffer (50 mM Tris-HCl, 100 mM DTT, 2% Sodium dodecyl sulfate (SDS), 0,1% bromophenol blue, 10% glycerol, pH 6.8). The samples were analyzed by SDS-PAGE to confirm the conditions for Httex1-37Q expression.

The large-scale expression of His₆-SUMO-Httex1-37Q was performed in 1L LB/Km at 16 °C, 180 rpm, and using 0.6 mM of IPTG. The cells were harvested by centrifugation at 8000 rpm, 10 min, and 4 °C and the pellet was resuspended in 60 mL of buffer A1 (50 mM Tris-HCl, 500 mM NaCl, 15 mM imidazole, pH 8.0), supplemented with 0.1 mM PMSF and 1 mini-tablet of protease inhibitors. The resuspended cells were stored at -80 °C until purification.

2.3.2. Purification of tag-free Httex1-37Q protein

Cells (from 1L growth cells) were first sonicated on ice using the Branson Sonifier 250 with 9 cycles of 15 pulses (duty cycle of 50% and an output control of 9-10) and 5 minutes of rest between each cycle. The cell lysate was centrifuged at 17 600 x g at 4 °C for 10 minutes and then for another 1 hour. The supernatant was then filtered through a 0.45 µm syringe filter (low protein binding) to remove any cell debris left.

First Approach

The His₆-SUMO-Httex1-37Q fusion protein was initially purified by an immobilized metal affinity chromatography (IMAC) performed in an ÄKTA Start System (GE Healthcare). Briefly, the filtered supernatant was loaded into a 5 mL HisTrap FF column equilibrated in Buffer A1 at a flow rate of 1.5 mL/min. The non-specific bound proteins were washed out with buffer A1 at a flow rate of 5 mL/min. The fusion protein was then eluted in a gradient of 5-100% buffer B (50 mM Tris-HCl, 500 mM NaCl, 500 mM imidazole, pH 8.0) at a flow of 1.5 mL/min and in 5mL fractions.

The fractions containing the His₆-SUMO-Httex1-37Q fusion protein were pooled and buffer exchanged to buffer C (50 mM Tris-HCl, 150 mM NaCl, 15 mM imidazole, pH 8.0) in an Amicon Ultra-15 3 kDa cutoff or using a 30 mL Slide-A-Lyzer 10 kDa MW cutoff dialysis cassette O/N at 4°C. To cleave the His₆-SUMO tag, the His₆-SUMO-Httex1-37Q fusion protein was incubated with ubiquitin-like protease 1 (ULP1) (containing a His₆-tag) protease in a volume ratio of 1:50 and 1mM of DTT for about 2.5 to 3 hours on a rotator at 4 °C. Samples were taken at each 30 minutes for SDS-PAGE analysis.

A second IMAC was performed to remove the His₆-SUMO tag and the His₆-ULP1 enzyme from the tag-free Httex1-37Q protein. The sample was then loaded into a 5 mL HisTrap FF column equilibrated with buffer C at 1.5 mL/min, and the tag-free Httex1-37Q protein was eluted in the flow-through at a flow rate of 2.5 mL/min in 2.5 mL fractions.

Second Approach

The cell lysis and the first IMAC were performed as described for the *first approach* with minor modifications. Specifically, the imidazole concentrations in the first IMAC were adjusted for Buffer A2 (50 mM Tris-HCl, 500 mM NaCl, pH 8.0- without imidazole) and Buffer B2 (50 mM Tris-HCl, 500 mM NaCl, 250 mM imidazole, pH 8.0). A second IMAC was also conducted, but here we used a 1 mL HisTrap FF column equilibrated with buffer C, in which the sample was applied at 1.5 mL/min and collected in 500 μ L fractions of the flow-through.

The protein concentration was determined using the Pierce™ Modified Lowry Protein Assay Kit the first time. The remaining times the Pierce™ BCA Protein Assay Kit was used. The fractions containing pure Httex1-37Q (100 μ L) were flash-frozen in liquid nitrogen for final storage at -80 °C.

2.4. Production of the His₆-SUMO-Httex1-43Q fusion protein

The His₆-SUMO-Httex1-43Q fusion protein was recombinantly expressed as detailed for Httex1-37Q variant (section 2.3.1): specifically, 1 L of culture was induced with 0.6 mM of IPTG and grown O/N at 16 °C and 180 rpm. However, for this pathogenic variant, the His₆-SUMO-tag was not removed during the purification procedure due to its high aggregation propensity. Therefore, Httex1-43Q was only purified in a fusion form and involved three major steps: (1) an initial IMAC, (2) buffer exchange and concentration for ~4 mL, and (3) several size exclusion chromatography (SEC) steps for final purification.

The cell lysis was performed as described for Httex1-37Q and the first IMAC was conducted using the *second approach* conditions (section 2.3.2). After the IMAC, fractions containing the His₆-SUMO-Httex1-43Q fusion protein were pooled and concentrated in SEC buffer (50 mM Tris-HCl, 200 mM NaCl, pH 8.0) with 5 mM DTT for about 4 mL using an Amicon Ultra-15 10 kDa cutoff. Between centrifugation runs, the sample was resuspended in the Amicon to prevent the formation of aggregates and adsorption to the membrane.

The His₆-SUMO-Httex1-43Q fusion protein was further purified by multiple SECs using a Superdex TM 75 10/300 GL column in an ÄKTA Purifying System (GE Healthcare). Briefly, for each SEC, 0.5 mL of sample was loaded into the column equilibrated in SEC buffer, at a flow rate of 0.3 mL/min and collecting 0.5 mL fractions. An SDS-PAGE gel was run to determine the fractions containing the highest pure / concentrated fusion protein. All these procedures were conducted in ice to prevent the protein aggregation.

The protein concentration was determined with the Pierce™ BCA Protein Assay Kit and storage (100 μ L at -80 °C) were performed as described above for Httex1-37Q (section 2.3.2).

2.5 SDS-PAGE gels

SDS-PAGE gels were performed between each Httex1 purification step. Briefly, 40 μL of sample were mixed with 20 μL of loading buffer and then denatured at 100 $^{\circ}\text{C}$ for 10 minutes. NZYColour Protein Marker II (NzyTech) was used as protein ladder. The samples were loaded into polyacrylamide gels (5% stacking and 15% resolving). Electrophoresis was performed first at 90 V for 10 minutes and then at 175 V for 50 minutes in the Mini-PROTEAN Tetra Vertical Electrophoresis Cell (Bio-Rad). The gels were final stained with Bluesafe.

2.6 Liposome Preparation

Large unilamellar vesicles (LUVs) composed of 25:75 POPC:POPS were prepared to evaluate the impact of anionic lipid membranes on Httex1-43Q aggregation. LUVs were obtained by extrusion as described in the literature [72]. Chloroform stock solutions of POPC and POPS previously prepared in the lab (with 18.69 mM and 17.49 mM, respectively) were mixed for obtaining a final lipid concentration of 0.5 mM. The chloroform was then evaporated using a stream of nitrogen and further under vacuum for at least 3 hours. The dry lipid was then resuspended in buffer F (50 mM Tris-HCl, 150 mM NaCl, pH 7.4). To form multilamellar vesicles (MLVs), the lipid mixture was submitted to 10 freeze-thaw cycles (in liquid nitrogen for 30 seconds and thaw at 50 $^{\circ}\text{C}$ for 1 minute and 30 seconds). To obtain LUVs, the lipid suspension was further extruded (for 31 times) through a 50-nm diameter polycarbonate membrane filter using an Avanti Mini-Extruder according to the manufacturer's instructions.

2.7 ThT fluorescence assays

ThT fluorescence assays were performed to detect amyloid fibril formation. These experiments were conducted in a PolarStar Optima microplate reader (BMG Labtech) using a 96-well microplates F-bottom and non-binding protein. Briefly, samples were measured for 16 hours at 25 $^{\circ}\text{C}$ and with 250 cycles of 230 seconds with 20 flashes per well, shaken for 20 seconds before each cycle, and with the measurement starting at 0.2 seconds. Shaking mode was double orbital with a shaking width of 4 mm. Scanning mode was orbital averaging with a scan diameter of 4 mm. The aggregation kinetics was monitored by measuring the fluorescence intensity (excitation 440-10 nm, emission 480-10 nm) and the gain was adjusted to 1375. The bottom optic was used to measure the fluorescence with a positioning delay of 0.2 seconds and a bidirectional, horizontal left to right, top to bottom reading direction.

Before each assay, protein samples previously stored at -80 $^{\circ}\text{C}$ were centrifuged at 12000 g for 2 minutes at 4 $^{\circ}\text{C}$ to remove large aggregates. We employed different strategies for Httex1-37Q and Httex1-43Q variants:

For Httex1-37Q: Purified tag-free Httex1-37Q (5, 10, 12.5, 20, 30, 50 μM) was incubated with 50 μM ThT in Buffer F. ThT in buffer and Buffer F were used as a control. The final volume for each well was 250 μL .

For the Httex1-43Q: For aggregation in solution, 50 μM ThT was incubated with 5, 10 and 15 μM of Httex1-43Q fusion protein, ULP1 and 1mM DTT in Buffer F. For evaluating the impact of anionic lipid membranes in Httex1-43Q aggregation kinetics, for ThT assays with 5 and 10 μM of fusion protein was also added 25 μM , 50 μM , 100 μM and 200 μM of LUVs 25:75 POPC:POPS. Here, we performed several controls: (i) ThT in buffer, (ii) ThT and the fusion protein (without ULP1 and DTT), (iii) ThT and ULP1, and finally (iv) ThT and LUVs. The final volume for each well was 250 μL .

The data obtained throughout the ThT fluorescence assays was treated using Excel (Microsoft Office) and the graphs were drawn using OriginLab software.

CHAPTER 3
RESULTS AND
DISCUSSION

3.1. Production of tag-free Httex1-37Q

3.1.1. Expression test of His₆-SUMO-Httex1-37Q

The pET-SUMO-Httex1-37Q plasmid was previously created in the host lab. Before cloning the plasmid was sent for sequencing, with positive results. However, the production of Httex1-37Q using this plasmid had not been tested.

In the scope of this thesis, we initially evaluated the expression of the His₆-SUMO-Httex1-37Q fusion protein in *E.coli* BL21(DE3) after induction with several IPTG concentrations at 16°C. The use of the SUMO-tag improves the solubilization of Httex1-37Q and avoids its toxicity for *E.coli*.

Figure 3.1-A shows the SDS-PAGE gel obtained from *E. coli* samples collected before and after induction with IPTG (0.4 mM, 0.6 mM, and 0.8 mM) or without IPTG (for auto-induction). The bands corresponding to the His₆-SUMO-Httex1-37Q fusion protein (between 35-48 kDa Molecular Weights (MW)) display similar intensities across the 0.4 mM, 0.6 mM, and 0.8 mM IPTG concentrations.

The results suggest that the protein was not expressed or is not significant before the addition of IPTG. To act in accordance with previous work in our lab for other Httex1 variants, 0.6 mM of IPTG was selected for the overexpression at large volumes.

3.1.2. Purification of the tag-free Httex1-37Q

Httex1-37Q was purified as tag-free protein and its purification involved several optimizations regarding the buffers/columns for IMAC. In the first approach, we used buffers A1 and B1 with high imidazole concentrations and included several purification steps: (i) a first IMAC with a 5 mL HisTrap column to purify the His₆-SUMO-Httex1-37Q fusion protein, (ii) dialysis for exchanging Buffer B to Buffer C to lower the NaCl and imidazole concentrations, (iii) incubation of the fusion protein with ULP1 to cleave the His₆-SUMO tag, and finally (iv) a second IMAC with a 5 mL HisTrap column to collect the tag-free Httex1-37Q in the flow-through.

Because Httex1 variants are susceptible to aggregation/degradation, the samples were always handled in ice. Just as other IDPs and aggregation-prone proteins, purifying Httex1 is highly challenging, and the work must be done with agility and efficiency to prevent aggregation as much as possible.

The SDS-PAGE gels obtained after each purification step are shown in Figures 3.1 B-D. We note that both fusion and tag-free Httex1-37Q run at high molecular weights in the SDS-PAGE gels. This has been also reported in the literature due to the high content in proline and glutamine residues (PRD domain and polyQ tract, respectively) and the intrinsically disordered features of Httex1.

In particular, the His₆-SUMO-Httex1-37Q fusion protein has a theoretical MW of 24.6 kDa (calculated in ProtParam), but in the gel it runs between 35 and 48 kDa. The His₆-SUMO tag alone runs between 11-17 kDa and its true molecular weight is closer to 12.4 kDa [73]. The tag-free Httex1-37Q fragment has 12.1 kDa, and its band in the SDS-PAGE gel appears at approximately 25 kDa (between 20 and 25 kDa).

In the first IMAC, the His₆-SUMO-Httex1-37Q fusion protein initially bound to the 5-mL HisTrap column due to the high affinity of the His₆-tag to the nickel column. The fusion protein was then eluted in the gradient with Buffer B1 in fractions 4-8 (Figure 3.1-B, band between 35-48 kDa). Here, the increase of imidazole concentration caused a detachment of the fusion protein from the column, as imidazole has higher affinity for nickel. We note that other proteins also bound non-specifically to the column and were then eluted with Buffer B1.

For Httex1-37Q variant, we decided to cleave the His₆-SUMO tag from the fusion protein to generate tag-free Httex1-37Q protein. The fractions 4-8 (Figure 3.1-B) containing the fusion protein were pooled together and submitted to a dialysis process for exchanging to Buffer C using a 30 mL Slide-A-Lyze™ Dialysis Cassettes of 10 kDa cutoff at 4 °C. This was performed to optimize the enzymatic activity of ULP1 by decreasing the concentrations of NaCl and imidazole in the buffer.

Upon incubation with His₆-ULP1 and DTT, the His₆-SUMO tag was cleaved, generating tag-free Httex1-37Q and His₆-SUMO in solution. The cleavage occurred as expected. As shown in Figure 3.1-C, sample at time 0' (red box, before adding ULP1) contained the fusion protein that ran between 35-48 kDa, while at time 30' the band corresponding to the fusion protein disappeared and simultaneously the bands corresponding to tag-free Httex1-37Q (green box) and His₆-SUMO (orange arrow) appeared.

Httex1-37Q migrates between 20-25 kDa and the His₆-SUMO tag is located close to 17 kDa. Notably, the cleavage of the SUMO-tag occurred rapidly as shown in Figure 3.1-C, in which after only 30 minutes most of the fusion protein was cleaved by ULP1. This results in the co-existing in solution of His₆-SUMO and tag-free Httex1-37Q .

The next step involved the purification of the tag-free Httex1-37Q protein from the His₆-ULP1 and the His₆-SUMO tag. Here, we used a 5-mL HisTrap column and the tag-free protein was eluted in the flow-through of the second IMAC. In this case, His₆-ULP1 and the His₆-SUMO tag remained bound to the nickel in the column, while tag-free Httex1-37Q was eluted. The SDS-PAGE gel obtained for the fractions of the flow-through (Figure 3.1-D) shows some contaminant proteins, since faint bands appear above and below the band corresponding to the tag-free Httex1-37Q protein (highlighted with a green box). Here, tag-free Httex1-37Q also runs between 20 and 25 kDa and the SUMO-tag runs at approximately 17 kDa. The fractions containing the fusion protein were pooled and concentrated to about 500 µL for performing a size exclusion chromatography (SEC).

Unfortunately, the protein was lost during the concentration in Amicons or during the SEC. This was concluded because the obtained samples after SEC were run in a SDS-PAGE gel (not included in this thesis) and it was not detected bands. This indicates that the purification in this last step was ineffective.

One possible explanation is that the concentration of tag-free protein in Amicons has triggered its aggregation that these aggregates were eluted right in the beginning of the process (in SEC, the larger

molecules run faster). Alternatively, it is also possible that a substantial amount of protein was lost through the purification or have absorbed to Amicons filters.

It is also possible that tag-free Httex1-37Q protein passed through the SEC column and was eluted, although in such small concentrations that it was not detected in SDS-PAGE gels. The samples from the SEC purification were not subjected to protein quantification, since the protein was lost or not in enough amount for performing the ThT fluorescence assays.

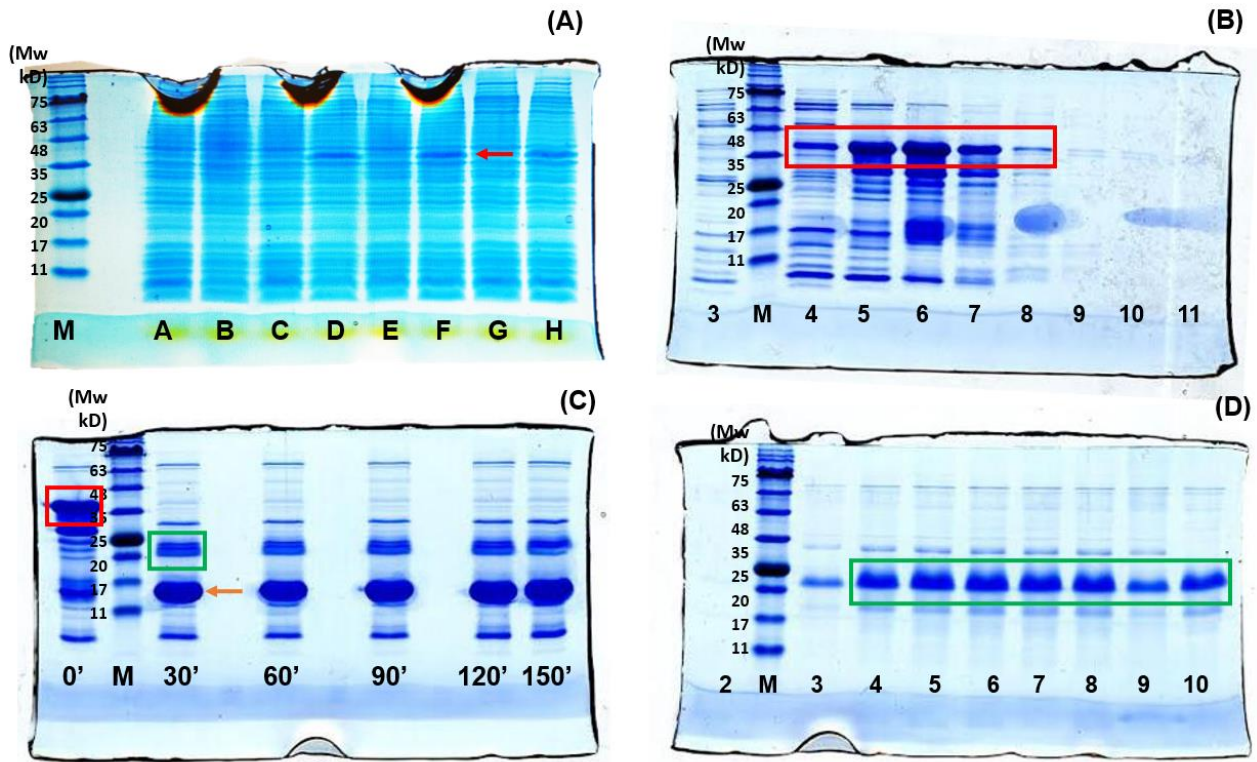


Figure 3.1: SDS-PAGE gels obtained in the first purification strategy for the Httex1-37Q protein. **(A)** The expression of the His₆-SUMO- Httex1-37Q protein in BL21 *E. coli* cells before (A, C, E and G) and after induction with IPTG with 0 mM (B), 0.4 mM (D), 0.6 mM (F) and 0.8 mM (H). The red arrow indicates the band corresponding to the His₆-SUMO-Httex1-37Q fusion protein and the IPTG concentration selected for the large overexpression. **(B)** Fractions of the gradient with Buffer B1 in the first IMAC; 3 – 11 represent the eluted fractions. The red box highlights the bands corresponding to the fusion Httex1-37Q protein. **(C)** Cleavage of the His₆-SUMO-Httex1-37Q fusion protein with ULP1 at different timeframes (30-minute intervals). 0', 30', 60' 90', 120', and 150' correspond to the collected timepoints. The red box represents the fusion protein at time 0. The green box highlights the tag-free Httex1-37Q protein. And the orange arrow indicates the SUMO-tag remaining in solution. **(D)** Fractions of the flow-through of the second IMAC; 3 – 10 represent the eluted fractions from the flow-through. The green box marks the location of the tag-free Httex1-37Q protein in the gel. In all SDS-Page gels, M indicates the markers (NZYColour Protein Marker II).

To avoid the concentration in Amicons of the tag-free Httex1-37Q, we optimized the previous protocol by: (i) decreasing the imidazole concentration in Buffer B2 to apply a more effective gradient and (ii) using a 1 mL HisTrap column for the second IMAC to not dilute the protein and to try to increase the final protein concentration.

The results obtained for the second approach are shown in Figure 3.2. This optimized process was employed several times, with similar results to the ones shown in Figure 3.1 being obtained.

In the first IMAC, Buffer B2 has 250 mM of imidazole and as expected, the His₆-SUMO-Httex1-37Q fusion protein (Figure 3.2 A-B, band at 35-48 KDa) was eluted in more fractions, namely fractions 4-14 were pooled together and prepared for cleavage.

Afterwards, the His₆-SUMO tag was cleaved by ULP1 and the results are shown in Figure 3.2-C. The protein was successfully cleaved, with results similar to the first strategy; at time 0', the fusion protein appears in the gel between 35-48 kDa, then after 30-minutes upon adding ULP1, most of the fusion protein was already cleaved by ULP1, resulting in two new bands corresponding to Httex1-37Q (between 20 and 25 kDa) and His₆-SUMO tag (approximately 17 kDa).

The results of the flow-through of the second IMAC containing the tag-free Httex1-37Q protein are displayed in Figures 3.2 D-E. It shows clear improvements comparing the previous approach (Figure 3.1-D), as there are fewer visible bands besides the band corresponding to the tag-free Httex1-37, located approximately at 20-25 kDa. This means that fewer contaminant proteins were present in the sample.

Removal of the His₆-SUMO tag from the fractions of interest was also successful, since the loaded sample (fraction F) shows at about 17 kDa an intense region that represents the tag. The eluted fractions in the flow-through (3-14) show no signal of the tag, meaning that the His₆-SUMO tag remained bound to the column throughout most of the elution process and it was only eluted in fraction 25 with 100 % Buffer B2. The protein concentrations of fractions 3-9 were determined by Lowry Protein Assay Kit, ranging 2.39 to 16.19 μ M.

Overall, this approach allowed to reduce the amount of protein lost in the process because less purification steps were performed, and more importantly we managed to avoid extensive protein aggregation in Amicons of tag-free Httex1-37Q.

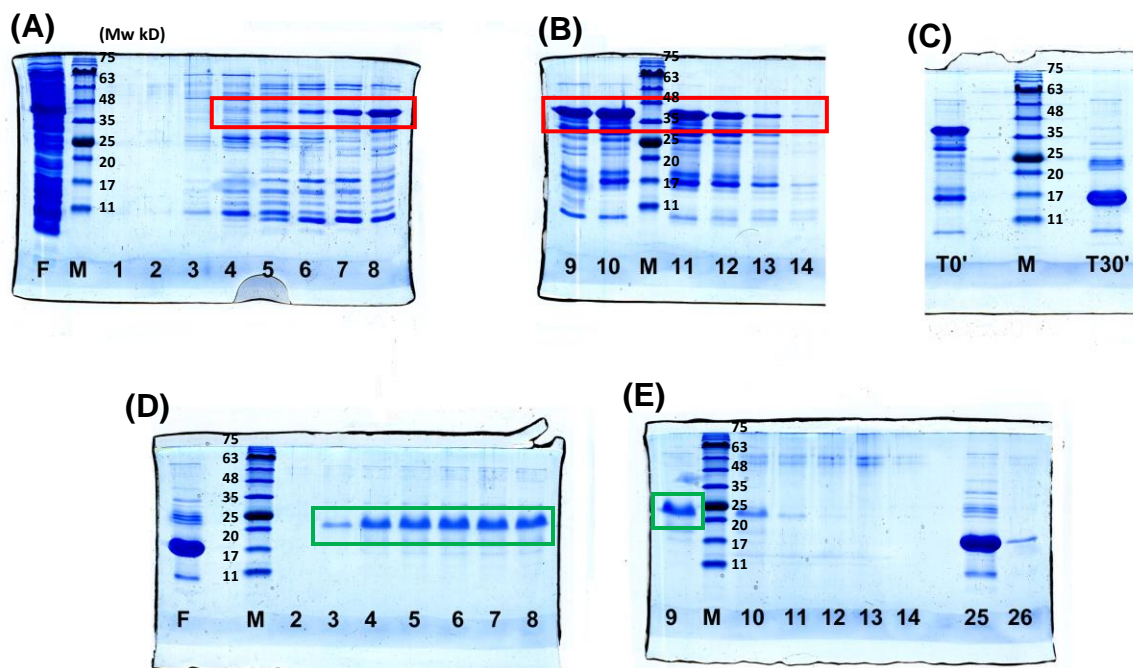


Figure 3.2: SDS-PAGE gels obtained in the optimized purification strategy for the Httex1-37Q protein. **(A) and (B)** First IMAC, where F – feed and 1-14 represent the collected fractions in the gradient with Buffer B2. In both gels, the red boxes highlight the location of the His₆-SUMO-Httex1-37Q fusion protein. **(C)** Cleavage of the His₆-SUMO tag from the fusion protein after adding ULP1 with samples taken at each 30 minutes. **(D) and (E)** Second IMAC for purification of tag-free Httex1-37Q from His₆-SUMO and the protease. F – feed; 2-14 and 25-26 represent the collected fractions. In all SDS-Page gels, M indicates the markers (NZYColour Protein Marker II).

3.2. ThT fluorescence assays of tag-free Httex1-37Q

After purifying the tag-free Httex1-37Q, we evaluated the formation of amyloid fibrils of this variant located at the threshold for pathological aggregation in HD by ThT fluorescence assays. In particular, ThT has been extensively used to monitor aggregation kinetics of Httex1 *in vitro* and other aggregation-prone proteins associated with neurodegeneration, such as α -synuclein (PD's), and amyloid- β peptide (AD's) [74]–[76]. This is because ThT binds to the β -sheet formation in amyloid fibers. The binding of ThT causes a conformational change in the molecule and it emits fluorescence.

ThT fluorescence assays were initially performed with 5, 10 and 12.5 μ M of tag-free Httex1-37Q in solution (Figure 3.3-A). The average and standard deviations of the ThT fluorescence intensities over all assays were also calculated and are shown in Table 3.1.

Firstly, for our control, the ThT fluorescence intensity in buffer (without protein) was constant and lower over the entire duration of the experiment (~16 hours), indicating that photobleaching did not occur. When

ThT was incubated with the tag-free Httex1-37Q, ThT intensity was always constant within our experiments and simultaneously above the control condition (Figure 3.3-A, Table 3.1). Moreover, the ThT fluorescence intensity increased with the protein concentration in the assay. More explicitly, for the results shown in Figure 3.3-A, the fluorescence intensity for 5 μM of protein was 2597 ± 31 , for 10 μM was 4383 ± 60 (and 4304 ± 57), and for 12.5 μM we obtained the highest value of fluorescence intensity (5092 ± 71) (Table 3.1). As binding of ThT to the β -sheet in amyloid fibrils results in the increase of ThT fluorescence, the data in both graphs reveal that the tag-free protein was already aggregated before starting the assay and that further aggregation did not occur during ~ 16 hours. If further aggregation had occurred, we would have seen an increase in ThT fluorescence intensity.

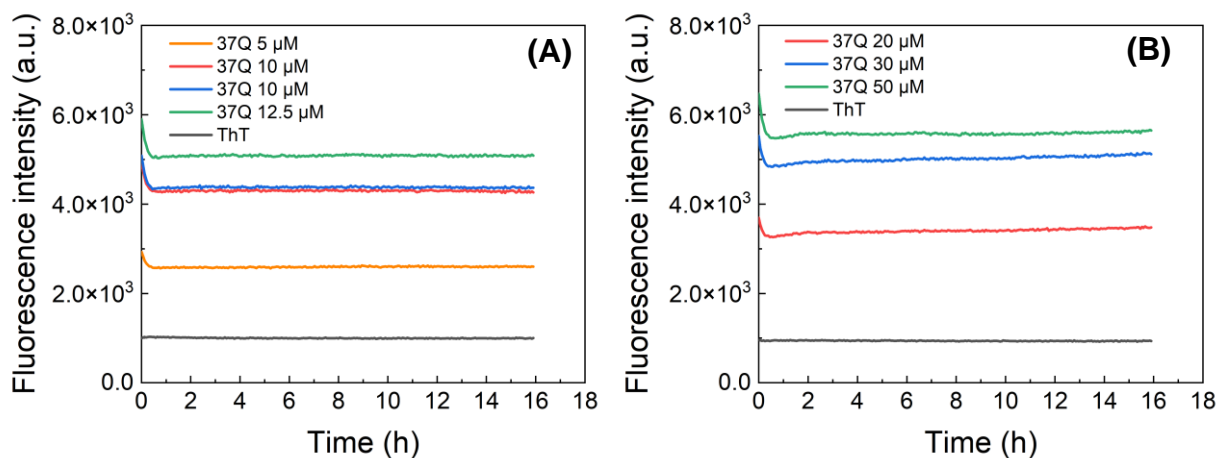


Figure 3.3: ThT fluorescence assays for monitoring the amyloid fibril formation of tag-free Httex1-37Q. **(A)** ThT fluorescence signal recorded upon incubation with distinct concentrations of Httex1-37Q: 5 μM (orange curve), 10 μM (red and blue curves), and 12.5 μM (green curve). **(B)** Higher Httex1-37Q concentrations were evaluated: 20 (red curve), 30 (blue curve), and 50 μM (green curve). The grey curves in both figures represent the control (only ThT in buffer F).

Table 3.1. Average (mean) and standard deviation (STDEV) of ThT fluorescence intensities upon incubation with tag-free Httex1-37Q for the data presented in Figure 3.3 (for ~ 16 hours).

| | 5 μM | 10 μM | 10 μM | 12.5 μM | 20 μM | 30 μM | 50 μM |
|--------------|-----------------|------------------|------------------|--------------------|------------------|------------------|------------------|
| Mean | 2597 | 4304 | 4383 | 5092 | 3401 | 5015 | 5584 |
| STDEV | 31 | 57 | 60 | 71 | 51 | 75 | 78 |

We still explored the amyloid fibril formation for longer times by measuring the ThT fluorescence of the previous samples after 29, 52 and 196 hours after starting the assay (Figure 3.3-A). For all protein concentrations explored, ThT fluorescence intensities did not change, showing that fibrillation already

attained is maximum at the beginning of the assay and indeed further aggregation did not occur. Table 2 shows the registered ThT fluorescence intensity values at the different time points.

Table 3.2. ThT fluorescence intensity values registered at 29, 52, and 196 hours after starting the aggregation kinetic assay.

| Time (h) | 5 μ M | 10 μ M | 10 μ M | 12.5 μ M |
|------------|-----------|------------|------------|--------------|
| 29 | 3049 | 5282 | 5360 | 6196 |
| 52 | 2931 | 4893 | 4972 | 5806 |
| 196 | 3172 | 4834 | 4994 | 6020 |

We further investigated high tag-free Httex1-37Q concentrations (Figure 3.3-B). Again, ThT fluorescence intensities within the experimental conditions were constant. The same trend described in Figure 3.3-A is observed for Figure 3.3-B, where the lowest concentration of protein (20 μ M) has the lowest average value of fluorescence intensity (3401 ± 51) and the highest concentration of protein explored (50 μ M) shows the highest average value of fluorescence intensity (5584 ± 78). For 30 μ M concentration was obtained an average fluorescence intensity of 5015 ± 75 .

It is important to note that buffer F was filtered before each measurement and also the protein samples retrieved from storage at -80 °C were thawed and submitted to a centrifugation step before each assay to remove any aggregates that could have formed. Therefore, our data support two hypotheses: (i) that the centrifugation was not efficient in removing the aggregates or (ii) the aggregation of the tag-free protein occurred too rapidly to be monitored.

The results obtained in this section of the project strongly suggest that the aggregation occurred shortly after SUMO-tag cleavage during the purification, which turns difficult to start the ThT assay with Httex1 as a free monomer.

Indeed, if there were free monomers in the sample, the ThT fluorescence values for monomers would have been very low and close to the control condition. Since that is not observed in the graphs, we infer that the most likely option is that the sample aggregated between the cleavage of the tag and preparation of the fluorescence assays.

Overall, the lack of a sigmoid curve for tag-free Httex1-37Q aggregation experiments suggests that aggregation occurred too quickly to be detected. The protocol used for isolation of Httex1-37Q fragments involved the cleavage of the His₆-SUMO tag from the fusion protein between the first and second IMAC, using ULP1 enzyme. This leaves a large time interval where the fragment is free and more prone for aggregation over time, for example, during the elution step of the second IMAC or until the samples are prepared for storage at -80 °C.

Although here we were not able to monitor the fibrillation of tag-free Httex1-37Q by ThT fluorescence, future studies should use the fusion construct and just cleave the SUMO-tag during the assay (following a similar approach used for Httex1-43Q, next section).

3.3. Production of the His₆-SUMO-Httex1-43Q fusion protein

Considering the results obtained for ThT fluorescence assays of tag-free Httex1-37Q (section 3.2), we decided to purify Httex1-43Q as a fusion protein, meaning that the His₆-SUMO tag was not cleaved during the purification processes. This variant was chosen specifically because its polyQ-length is considered pathological and causes HD. Since this fragment has a larger number of glutamines in the polyQ domain, it is more prone to aggregation than Httex1-37Q.

The purification of the His₆-SUMO-Httex1-43Q fusion protein included: 1) an IMAC, 2) buffer exchange and concentration to 4 mL in Amicons, and finally 3) several SECs (each with 0.5 mL of loaded sample) as the final purification step. Concentration of purified protein was determined using the Pierce™ BCA Protein Assay Kit. The strategy followed was to not cleave the SUMO tag between purification steps, but to only add the ULP1 protease during the preparation of the ThT fluorescence assays.

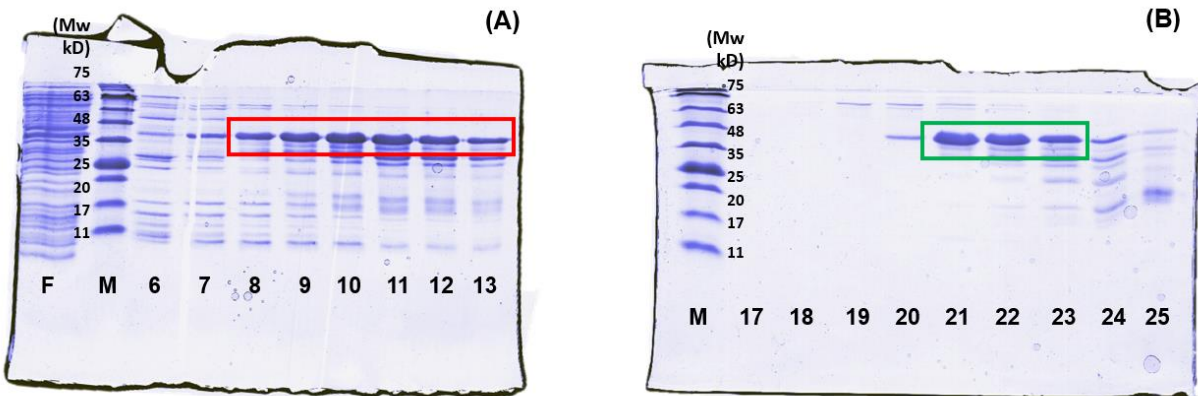


Figure 3.4: SDS-PAGE gels obtained for the purification of His₆-SUMO-Httex1-43Q fusion protein. **(A)** IMAC; F – feed and 6-13 represent the collected fractions during the gradient with Buffer B2. The red box highlights the location of fusion protein and the fractions 8-13 were selected for pooling and concentration. **(B)** Fractions 17-25 collected during the SEC. The red box highlights the fractions that were then analyzed regarding their protein concentration and stored at -80°C for further experiments. M represents the markers (NZYColour Protein Marker II).

The results obtained from the IMAC and a typical SEC are shown in Figure 3.4. It is important to note that Httex1-43Q, just as the 37Q variant, appears to run at higher molecular weights in the SDS-PAGE gels

due to its intrinsically disordered nature, as well as high content in proline and glutamine residues. The true molecular weight of His₆-SUMO-Httex1-43Q (calculated in ProtParam) is 25.4 kDa.

In the first IMAC (Figure 3.4-A), the His₆-SUMO-Httex1-43Q fusion protein runs between 35 and 48 kDa. The fractions 8-13 (highlighted by the red box) were selected for further purification. Overall, the gel shows satisfactory results with bands of high intensity for the fusion protein, despite the presence of other contaminant proteins represented by bands above and below the protein of interest. These fractions were pooled together and then concentrated until a volume of 4 mL using 10 kDa cutoff Amicons.

Several SEC were performed using 0.5 mL of the previous concentrated sample. One of the results is shown in Figure 3.4-B, where we observe that the fusion protein was relatively pure in fractions 21-23 (between 35 kDa and 48 kDa). These fractions were submitted to Pierce™ BCA Protein Assay Kit to determine the protein concentration. The typical total protein concentrations ranged 20 – 50 μM. Looking at the results obtained in the SDS-PAGE gels, we assume that most of that concentration corresponds to His₆-SUMO-Httex1-43Q.

3.4. ThT fluorescence assays of Httex1-43Q

3.4.1. Fibrillation of Httex1-43Q in solution

Fibrillation of tag-free Httex1-43Q

ThT fluorescence assays were initially performed with tag-free Httex1-43Q. The protein was purified using the second approach purification of Httex1-37Q. The results are shown in Figure 3.5 and Table 3.3 indicate the average ThT fluorescence intensity values and standard deviation obtained over the assay.

Globally, we obtained here similar ThT intensity profiles to those registered for tag-free Httex1-37Q (Figure 3.3). All the samples with tag-free protein explored show ThT fluorescence values above the control condition, (ThT only in solution). Again, the ThT fluorescence intensity was constant within each experimental condition and increased with the protein concentration.

Specifically, we initially explored 10 and 15 μM of Httex1-43Q protein and obtained average intensities of 2290 ± 65 and 3594 ± 83 , respectively. Afterwards, we repeated the assay with the same concentrations (average intensities of 5237 ± 144 for 10 μM and 7181 ± 218 for 15 μM) and explored a higher Httex1-43Q concentration of 48 μM (average intensity of 15669 ± 398). However, even for 48 μM of tag-free Httex1-43Q, the ThT fluorescence intensity remained constant, and a higher value was recorded.

Together, these results reveal that tag-free Httex1-43Q is already aggregated before starting to measure the ThT fluorescence intensities.

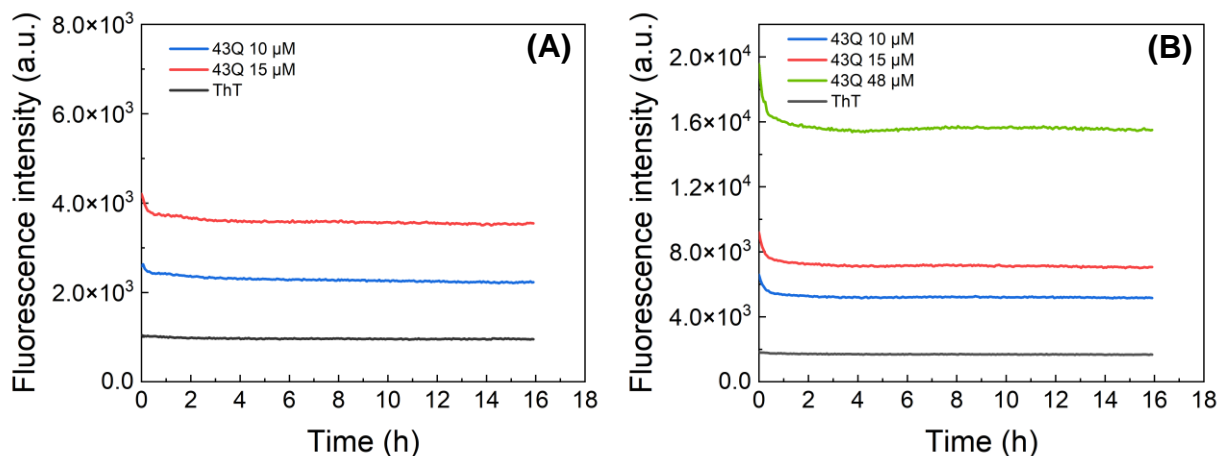


Figure 3.5: ThT fluorescence assays for tag-free Httex1-43Q in solution. ThT fluorescence intensities upon incubation with **(A)** 10 and 15 μM and **(B)** 10, 15, and 48 μM of tag-free Httex1-43Q. In both figures, ThT intensity in buffer was used as a control. The results of tag-free Httex1-43Q fluorescence assay show the same profile that those obtained for tag-free Httex1-37Q.

Table 3.3. Average (mean) and standard deviation (STDEV) of ThT fluorescence intensities obtained upon incubation with tag-free Httex1-43Q for the data presented in Figure 3.5 (for ~ 16 hours).

| | 10 μM (A) | 10 μM (B) | 15 μM (A) | 15 μM (B) | 48 μM |
|----------------|-----------|-----------|-----------|-----------|-------|
| Average | 2290 | 5237 | 3594 | 7181 | 15669 |
| (STDEV) | 65 | 144 | 83 | 218 | 398 |

Fibrillation of His₆-SUMO-Httex1-43Q fusion protein

The results presented here were performed with His₆-SUMO-Httex1-43Q fusion protein obtained after SEC (Figure 3.4). The His₆-SUMO tag was only cleaved upon addition of ULP1 enzyme in the wells and before ThT fluorescence was measured. We note that according to our results and also previous preliminary data in the host lab, the SUMO-tag cleavage occurs too quick and almost immediately upon incubation with ULP1, allowing that the cleavage of the solubilizing tag has a minor impact on Httex1-43Q aggregation profile. A few minutes after the addition of ULP1 in the microplate well, the tag is cleaved and Httex1-43Q is free and in a monomeric state.

The fibrillation of Httex1-43Q in solution was initially studied by incubation of ThT with the His₆-SUMO-Httex1-43Q fusion protein and also adding ULP1 and DTT. Two different fusion concentrations were tested: 5 μM and 10 μM. It is important to note that Httex1-43Q fragment is within a range of HD pathogenicity, with a near certain possibility of causing onset of the disease. A Httex1 fragment with 43Q

is more prone to aggregation than with 37Q, so it is expected that Httex1-43Q will aggregate at lower concentrations and it would be detected by ThT fluorescence.

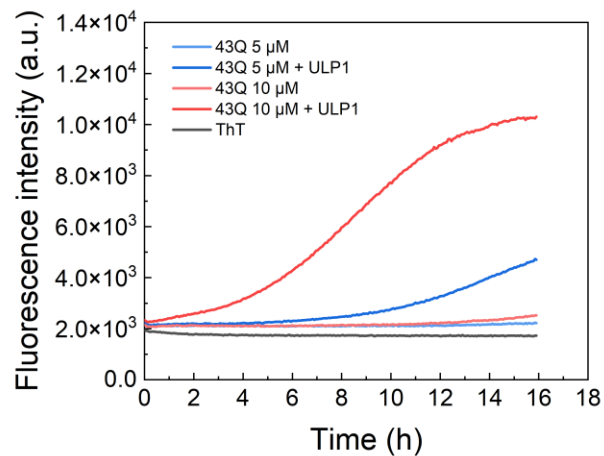


Figure 3.6: ThT fluorescence assays for Httex1-43Q. ThT fluorescence intensities were recorded upon incubation with 5 μM and 10 μM of Httex1-43Q fusion protein and also ULP1 and DTT. Control conditions include: ThT in buffer and also ThT with the fusion protein (without the protease).

Again for ThT in buffer, its fluorescence intensity was very low and constant over the experiment. For ThT with 5 μM of the Httex1-43Q fusion protein (without ULP1), its fluorescence intensity was slightly above the control condition throughout the entire duration of the assay.

In the case of 10 μM Httex1-43Q fusion protein without ULP1, for most of the duration of the experiment, the fluorescence levels remained constant. Only towards the final 2 hours of the experiment, the fluorescence intensity values started slowly increasing. This suggests that the protein has started to form amyloid fibers that ThT can bind to and its fluorescence increased. Therefore, the propensity of the pathological Httex1 fragments to aggregate and form fibers is very strong. Even in the presence of the solubilizing tag, which is supposed to help keep the protein stable, aggregation seems to occur.

In addition, Figure 3.6 shows that for all experimental conditions, the fluorescence intensities recorded at the very beginning of the assay were similar. This supports the hypothesis that incubating ULP1 with Httex1 fusion variants during the ThT fluorescence assay allows for a clean experiment, where all conditions have approximately the same starting point (cleavage of the tag) and thus making the obtained kinetic data more significant.

For conditions with addition of ULP1 for SUMO tag cleaved, an increase in ThT fluorescence was detected. These conditions have the same starting point and register practically the same fluorescence intensity at the beginning of the experiment (around 2200 intensity). However, after some hours, the

fluorescence intensity values started to increase, strongly suggesting the formation of amyloid fibrils detected by ThT.

There is also a notable difference in the curve profiles of 5 and 10 μM concentrations. For 5 μM of fusion protein and ULP1, the increase of ThT fluorescence happens very slowly over time, and only towards the end of the experiment it begins increasing at faster rates, even though never coming close to a plateau during our experiment (16 hours). It is possible that the protein concentration is so small that the aggregation process (the lag phase and exponential growth phase) is stretched over time. For 10 μM of fusion protein and ULP1, a more typical sigmoid curve was obtained. The initial fluorescence value started close to the control condition and then steadily increased over time. Towards the end of the experiment, ThT fluorescence reached almost the plateau phase (around 10 000 intensity).

In summary, these results confirm that studying the aggregation kinetics of previously cleaved and purified tag-free Httex1 fragments is extremely difficult. Significant results are obtained using a fusion construct and just cleave the SUMO-tag at the beginning of the assay.

3.4.2. Fibrillation of His6-SUMO-Httex1-43Q with lipid vesicles

Experiments were performed by incubating ThT with the fusion protein, ULP1 and DTT and further adding LUVs composed of 75:25 POPS:POPC. The main goal was to evaluate the impact of anionic lipid membranes in Httex-43Q fibrillation.

Initially, the assays were carried out with 5 μM of His₆-SUMO-Httex1-43Q fusion protein and different concentrations of LUVs, namely 25 μM , 50 μM , and 100 μM . ULP1 was also added during the preparation of the ThT fluorescence assay, initiating the cleavage of the His₆-SUMO tag. To better evaluate the Httex1-43Q fibrillation, we extended the assay for 21 hours.

Figure 3.7-A shows the corrected fluorescence intensity values for the respective control. For the samples with only protein, the ThT fluorescence intensities in buffer were subtracted and for the samples with lipid the values for ThT with LUVs were discounted. Figure 3.7-B shows the values of the control conditions alone.

First, all tested conditions show fluorescence values above the simple control condition (ThT only in solution), and as expected ThT fluorescence in buffer was also constant throughout the experiment (around 2000 intensity) (Figure 3.7-B). The controls containing ThT and 25 or 50 μM of LUVs show constant values that are similar to the ThT intensity in buffer (around 2000, Figure 3.7-B). For the control with 100 μM of LUVs slightly higher values of ThT fluorescence intensity were recorded (around 2500, Figure 3.7-B). This is important because it allows us to conclude that ThT does not bind to LUVs in a significant manner, so essentially the ThT fluorescence signal can be attributed to the formation of amyloid fibers. It is important to note that these controls are not usually presented in the literature.

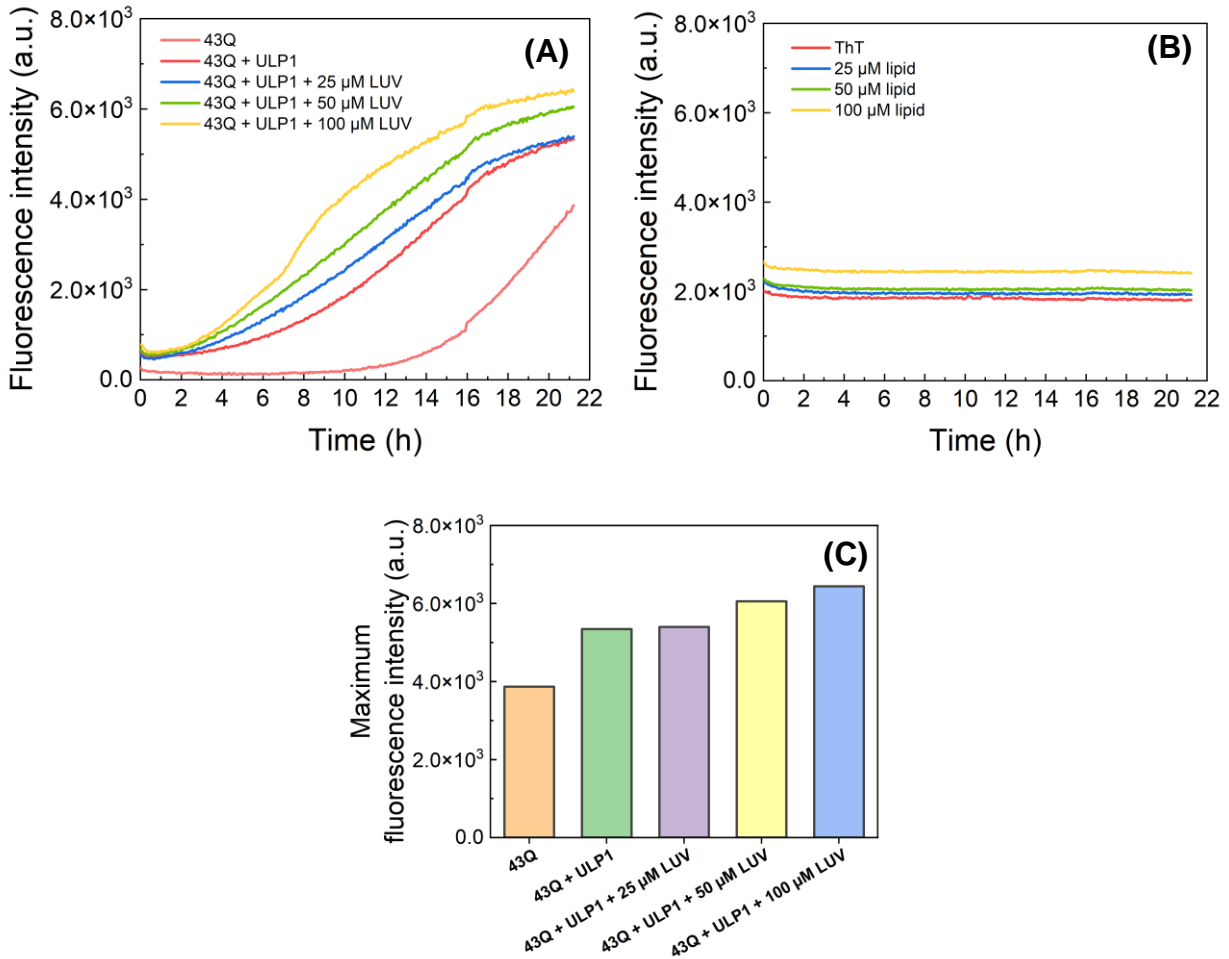


Figure 3.7: ThT fluorescence assays for 5 μ M Httex1-43Q with anionic lipid vesicles. **(A)** ThT fluorescence intensities obtained with 5 μ M of His₆-SUMO-Httex1-43Q fusion protein without ULP1 (without tag-cleavage); or with ULP1 (for tag-cleavage) in solution and in the presence of 25 μ M, 50 μ M or 100 μ M LUVs 25:75 POPC:POPS. The data were corrected by subtracting the corresponding averaged control intensity. **(B)** Control conditions for the ThT fluorescence assays. The controls consist of ThT in buffer (ThT), and ThT with 25 μ M, 50 μ M or 100 μ M of LUVs. **(C)** Bar graph illustrating the maximum fluorescence intensity at the end of the ThT assay for the experimental conditions represented in (A).

The conditions of Httex1-43Q with no lipid are similar to the previous results: His₆-SUMO-Httex1-43Q fusion protein with or without ULP1 still aggregated. The aggregation of His₆-SUMO-Httex1-43Q cannot be fully stopped, but its kinetic profile is slower and delayed when compared to the sample where the tag was removed. Only after 10 hours, the ThT fluorescence for the fusion protein started to increase. At the end of the experiment, the ThT fluorescence with the fusion protein was still increasing and showing no signs

of reaching a plateau. For the fusion protein incubated with ULP1, the increase in ThT fluorescence occurred much faster (after only 2 hours), however it did not reach a plateau either.

ThT fluorescence intensities obtained with 5 μM of His₆-SUMO-Httex1-43Q fusion protein with ULP1 and LUVs show a similar pattern to the His₆-SUMO-Httex1-43Q with ULP1 and without the LUVs. Despite the slow aggregation kinetics, it is possible to infer from the experimental data obtained with Httex1-43Q and LUVs that anionic lipid membranes affect Httex1-43Q aggregation.

Testing higher concentrations of His₆-SUMO-Httex1-43Q will allow us to further explore this effect. For the three lipid concentrations explored here (25, 50, and 100 μM of LUVs), fluorescence values were above control levels and also above Httex1-43Q in solution (both cleaved and non-cleaved). There also seems to be a direct effect of lipid concentration on aggregation, as higher lipid concentrations show higher fluorescence intensity values.

Figure 3.7-C compares the maximum fluorescence intensity between the different experimental conditions at the end of the experiment. These ThT fluorescence values increased with the lipid concentration in the assay. The maximum registered fluorescence values are as following: 5399 for 25 μM of LUVs, 6056 for 50 μM of LUVs, and finally 6441 for 100 μM of LUVs. Also, for Httex1-43Q without lipids, the following maximum fluorescence values were registered: 3867 for His₆-SUMO-Httex1-43Q, and 5342 for tag-free Httex1-43Q.

We next explored a high concentration of His₆-SUMO-Httex1-43Q fusion protein. Specifically, we applied the same strategy as before. ThT fluorescence assays were carried out with 10 μM of His₆-SUMO-Httex1-43Q fusion protein without ULP1; and also with ULP1 in solution and different LUV concentrations (50 μM , 100 μM , and 200 μM). The results of the assay are shown in Figure 3.8. We note that our control experiments show similar trends to the previous assay. ThT fluorescence in buffer is constant over time and with LUVs it slightly increased (but is not significant comparing with samples with protein).

Figure 3.8-A shows that the aggregation of the fusion protein (without ULP1) still occurred but with a slower kinetics; the fluorescence intensities remained constant in the first 8 hours and then increased, but a plateau was not reached in our experiment. This indicates that it is likely that even with solubilizing tags, the Httex1-43Q fragment is still prone to fibril formation and that the tag only delays the process. When the fusion protein's tag was cleaved from the protein (by addition of ULP1), the lag phase was much shorter and after approximately 1 hour the fluorescence started increasing in an exponential manner. A plateau of fluorescence was reached at about 14 hours after starting the experiment (11 100 intensity).

This reveals that the removal of the solubilizing tag has a significant effect on the Httex1-43Q fibrillation, as expected.

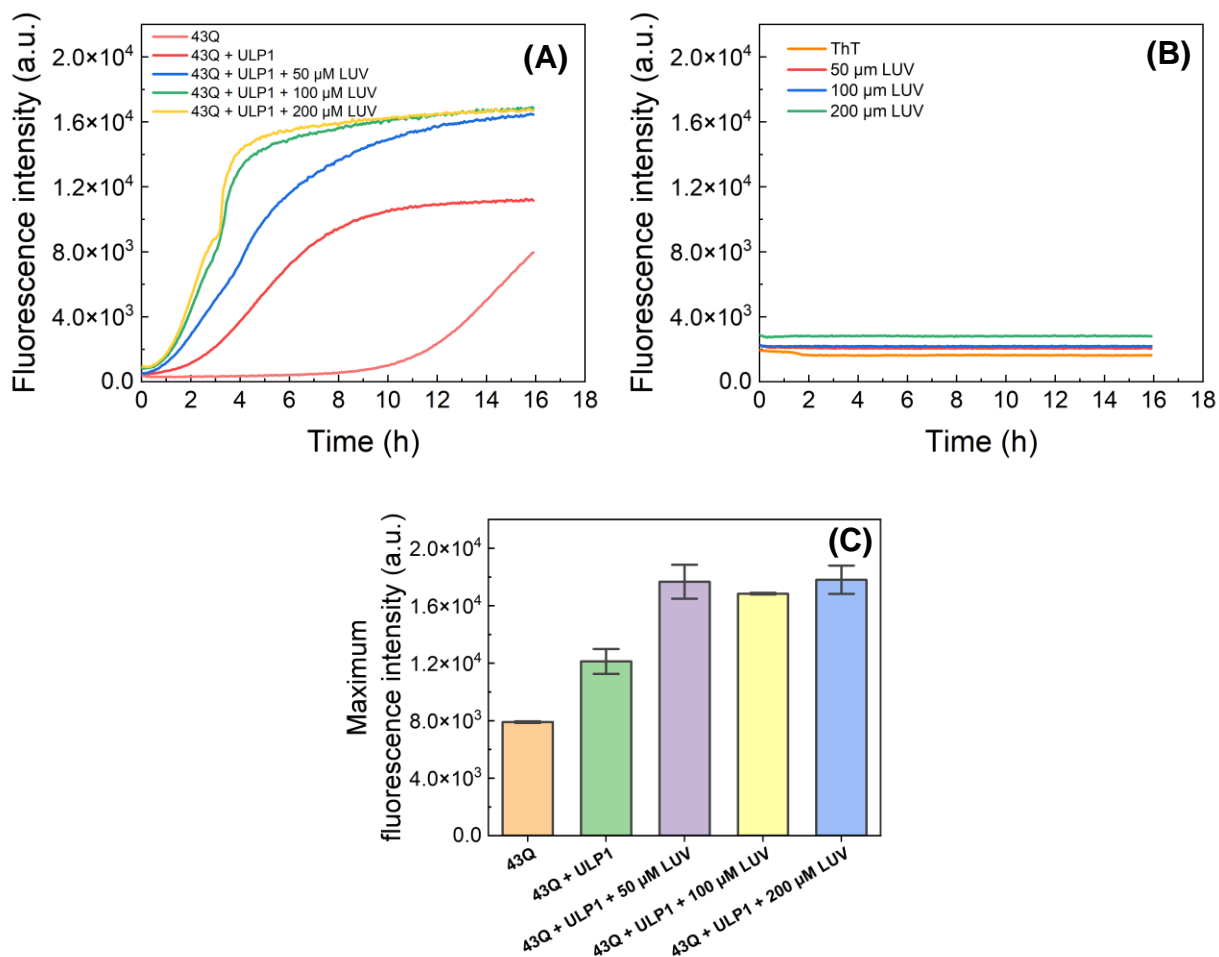


Figure 3.8: ThT fluorescence assays for 10 μM Httex1-43Q with anionic lipid vesicles. **(A)** ThT fluorescence intensities obtained with 10 μM of His₆-SUMO-Httex1-43Q fusion protein without ULP1 (without tag-cleavage); or with ULP1 (for tag-cleavage) in solution and in the presence of 50 μM , 100 μM or 200 μM LUVs 25:75 POPC:POPS. The data were corrected by subtracting the corresponding averaged control intensity. **(B)** Control conditions for the ThT fluorescence assays. The controls consist of ThT in buffer (ThT), and ThT with 50 μM , 100 μM or 200 μM of LUVs. **(C)** Bar graph illustrating the maximum fluorescence intensity at the end of the ThT assay for the experimental conditions represented in (A).

The graphs also illustrate the significant effect of lipid membranes on the aggregation of Httex1-43Q. It is seen in Figure 3.8-C that the difference of maximum fluorescence between those conditions and the conditions containing only Httex1-43Q and ThT (and ULP1 and DTT) are significant, with a difference of about 5500 between the Httex1-43Q with LUV and cleaved Httex1-43Q.

The aggregation kinetics of Httex1-43Q in the presence of lipid membranes were faster than in solution (Figure 3.8-A). They also show a typical sigmoid curve profile associated with amyloid fibril formation. For

100 μM and 200 μM lipid, ThT fluorescence reached a plateau phase at 4 hours, and for 50 μM of lipid only seems to approach a plateau at 12 hours.

In addition, our data supports that the extension of Httex1-43Q fibrillation was higher in the presence of anionic lipid membranes than in solution, since the ThT fluorescence intensities at the plateau were higher for samples with lipid (Figure 3.8-C). Considering that all samples contain the same protein concentration and only the lipid concentration was altered, we can conclude that anionic lipids have a high impact in Httex1-43Q aggregation.

3.5. Discussion

HD is a fatal and inherited neurodegenerative disease caused by the pathological expansion of the polyQ tract (above 37Q) within exon-1 of Htt protein [27]. Several evidence supports that biological membranes promote Httex1 aggregation and simultaneously these aggregates also cause membrane disruption and permeabilization, resulting in organelle dysfunction [77].

In addition, the physical and chemical properties of lipids heavily influence its membrane interaction and mechanism of aggregation [17], [67]. Ultimately, the rearrangement of these toxic fragments that promote aggregation *in vivo* can also lead to deposition within tissues and cellular organelles.

The detailed description of the molecular mechanism of Httex1 aggregation is crucial for understanding its pathological contribution for HD and may lead to the development of new strategies for HD treatment. Early studies relied on the use of synthetic polyQ peptides (with extra lysine residues) for solubilization. However, recent studies support that both flanking polyQ regions – Nt17 and PDR – modulate Httex1 aggregation in solution or in the presence of lipid membranes [45], [71], [78], [79].

Therefore, it is crucial to perform Httex1 aggregation assays in the context of the full-length fragment. More recently, several labs have developed ThT fluorescence assays with Httex1 fusion constructs (for solubilization) and performing only the tag-cleavage during the experiment [17]. However, their inter-comparison is highly challenging due to the use of distinct fusion constructs and proteases. Some data lack confirmation that Httex1 is in a monomeric state at beginning of these assays and the kinetics of tag-cleavage does not impact or delay Httex1 fibrillation.

The expression/purification and aggregation studies of Httex1 are extremely challenging due to its hydrophobic, intrinsically disordered, and aggregation-prone nature [7]. Therefore, several strategies have been developed for the recombinant expression in *E.coli*. They include the use of solubilizing-fusion tags, such as Glutathione S-Transferase (GST), Maltose Binding Protein (MBP), Thioredoxin [61].

In this thesis, we used a SUMO-fusion strategy that generates native tag-free Httex1 without extra amino acid residues after cleavage with ULP1 protease. Specifically, we focused on Httex-37Q and Httex-43Q variants and their fibrillation were evaluated by ThT fluorescence assays.

Production of tag-free Httex-37Q and ThT fluorescence assays

We initially optimized a strategy for obtaining tag-free Httex1-37Q. This variant was chosen because its polyQ-length is located at the threshold for pathological aggregation [27]. The plasmid was previously cloned in the lab and the expression and purification procedures were optimized in this thesis. An optimized protocol that comprises only IMACs and avoid concentration of tag-free protein in Amicons/or SECs was developed.

ThT fluorescence assays for evaluating aggregation of tag-free Httex1-37Q in solution were then performed. Briefly, the ThT fluorescence intensities with tag-free protein were constant throughout the duration of the assay (~16 hours) and always above the control condition (ThT only in buffer). There was no sigmoid curve or fluorescence increase observed. Moreover, the ThT fluorescence increased with the total protein concentration in the assay.

Together, these results suggest that fibril formation occurred before starting the assay and further aggregation did not occur. Furthermore, measuring the fluorescence of the sample at different times after the experiment and obtaining the same values of fluorescence intensity further solidifies this hypothesis. As described in literature, the native structure of Httex1 fragments and their physicochemical properties make them intrinsically disordered and highly unstable [46], [80] and thus are highly prone to aggregate.

These results are not usually obtained in literature, as researchers work with fusion proteins and proteases that cleave the solubilizing tag are used during fluorescence assays. In this thesis we attempted working with tag-free Httex1-37Q protein to eliminate the influence of the tag.

Production of Httex1-43Q fusion protein and ThT fluorescence assays

Httex1-43Q was purified as a fusion construct containing at the N-terminal a His₆-SUMO tag. Httex1-43Q comprises 43 glutamine residues within the polyQ region, making it an unstable protein and prone to aggregation and fibrillation. This specific variant was chosen because it is within a range considered a mutant protein that causes HD.

We decided to work with this protein as a fusion protein. The tag was not cleaved at any point during the purification. Only during the preparation of the ThT fluorescence assays, we added ULP1 to the wells to promote the tag-cleavage. It allows keeping the protein more stable and prevents its premature aggregation throughout the purification process. This tag-cleave during the ThT fluorescence assay should have minor effects in the aggregation kinetics, because ULP1 is extremely effective and fast at cleaving the His₆-SUMO tag. This suggests that in little time, there is a high concentration of free monomer to associate and begin the fibril formation process.

However, we note that different laboratories used different solubilization tags and consequently different proteases. This introduces a level of variability among laboratories that makes data comparison more challenging.

Several studies have also shown the importance of the flanking regions for both aggregation and lipid interactions. More specifically, Nt17's domain is responsible for membrane anchoring [70, p. 17], [81].

The choice to include lipids in this project comes from Httex1 fragment interacting with lipid membranes *in vivo*, and that these lipid membranes potentiate the aggregation and fibrillation process [18]. TBLE bilayers is a common model for membranes, especially because it is of biological origin, but its composition is complex, and it is difficult to evaluate the effect of individual lipids. In this thesis, we evaluated the impact of anionic lipid membranes by using LUVs composed of a mixture of zwitterionic lipids (POPC) and anionic (POPS) lipids.

ThT fluorescence assays were performed with two different concentrations of His₆-SUMO-Httex1-43Q (5 and 10 μ M) in conjunction with distinct concentrations of LUVs. When very low concentrations of protein were evaluated (5 μ M, Figure 3.7), the aggregation kinetics occurred slowly throughout the 21 hours of ThT fluorescence assay. None of the experimental conditions had shown signs of approaching a well-defined plateau, even when incubated with LUVs.

For a concentration of 10 μ M (Figure 3.8), a sigmoid curve profile can be observed for most conditions. The results obtained from the experiments show that anionic lipids promoted a faster aggregation rate for Httex1-43Q fibrils and that this happens in a concentration dependent manner. The aggregation kinetics is much faster when compared to the 5 μ M of Httex1-43Q condition, because a plateau was reached for all the conditions containing LUVs. In addition, the extension of fibrillation was higher in the presence of anionic LUVs than in solution.

While this data alone collected by fluorescence spectroscopy solidifies the idea that aggregation of mutant huntingtin follows a sigmoid curve model already backed by literature, there is nothing to be concluded about the morphology of the amyloid fibrils. ThT aggregation assay allows for the quantitative detection of amyloid fibers over time, but structural data would only be obtained by imaging techniques such as AFM and TEM [17], [18].

CHAPTER 4

CONCLUSION

4. Conclusion

Amyloidogenic intrinsically disordered proteins are exceptionally susceptible to degradation and aggregation, and thus extremely difficult to purify and work with. Previous research relied on the use of synthetic polyQs to study the effects of aggregation, but recently the importance of the flanking polyQ domains of Httex1 has been highlighted. This requires techniques that are efficient in expressing and producing this fragment to obtain information that is closer to the *in vivo* models. To accomplish this, studies have fused the Httex1 fragment to solubilize protein tags. However, these methods have some debilitating disadvantages: (i) cleavage may introduce new amino acids, (ii) due to the tags' large size monitoring small changes becomes complicated, and (iii) the presence of the tags might alter the aggregation properties.

The first two problems have not been observed with the use of SUMO tag. While ULP1 is required to cleave the tag from the Httex1-37Q fragment, the results also show that the enzyme is very efficient in doing so and it leaves most of the sample containing tag-free Httex1 fragments.

Furthermore, the influence of anionic lipids was evaluated in this project using fusion protein His₆-SUMO-Httex1-43Q. As literature has suggested, lipid membranes influence Httex1 aggregation and fibrillation mechanisms by potentiating the process [17], [69], [71]. Such phenomenon has also been observed in the results of this project for the full-length Httex1 fragment, where we see that Httex1 aggregates faster and shows higher fluorescence intensity in the presence of LUVs in a concentration-dependent manner.

4.1. Further Studies

Future studies should include the characterization of Httex1-37Q fibrillation by ThT fluorescence assays using a fusion construct as applied here to Httex1-43Q variant. Moreover, having established that anionic lipid membranes play a very important role in the aggregation process of Httex1-43Q, the next steps would be to further investigate more complex lipid compositions with co-existing of phase separation. The amyloid fibers should also be characterized morphologically by Atomic Force Microscopy (AFM) and Transmission Electron Microscopy (TEM).

To follow early steps of aggregation and not only detect amyloid fibrils as ThT reports, Httex1 could be engineered for introducing a cysteine and then site-specifically labeled with a thiol-reactive fluorophore (such as Atto 488 or Alexa 488) to perform anisotropy measurements. Moreover, site-specific labeling at each flanking polyQ domain could provide information of the role of each region in the Httex1 aggregation.

Bibliography

- [1] H. A. Lashuel, 'Rethinking protein aggregation and drug discovery in neurodegenerative diseases: Why we need to embrace complexity?', *Curr. Opin. Chem. Biol.*, vol. 64, pp. 67–75, Oct. 2021, doi: 10.1016/j.cbpa.2021.05.006.
- [2] C. A. Ross and M. A. Poirier, 'Protein aggregation and neurodegenerative disease', *Nat. Med.*, vol. 10, no. S7, pp. S10–S17, Jul. 2004, doi: 10.1038/nm1066.
- [3] F. Chiti and C. M. Dobson, 'Protein Misfolding, Amyloid Formation, and Human Disease: A Summary of Progress Over the Last Decade', *Annu. Rev. Biochem.*, vol. 86, no. 1, pp. 27–68, Jun. 2017, doi: 10.1146/annurev-biochem-061516-045115.
- [4] G. M. Shankar *et al.*, 'Amyloid- β protein dimers isolated directly from Alzheimer's brains impair synaptic plasticity and memory', *Nat. Med.*, vol. 14, no. 8, pp. 837–842, Aug. 2008, doi: 10.1038/nm1782.
- [5] E. B. Johnson and S. Gregory, 'Huntington's disease: Brain imaging in Huntington's disease', in *Progress in Molecular Biology and Translational Science*, vol. 165, Elsevier, 2019, pp. 321–369. doi: 10.1016/bs.pmbts.2019.04.004.
- [6] S. Iuchi, G. Hoffner, P. Verbeke, P. Djian, and H. Green, 'Oligomeric and polymeric aggregates formed by proteins containing expanded polyglutamine', *Proc. Natl. Acad. Sci.*, vol. 100, no. 5, pp. 2409–2414, Mar. 2003, doi: 10.1073/pnas.0437660100.
- [7] L. Jia *et al.*, 'Expression and purification of amyloid β -protein, tau, and α -synuclein in *Escherichia coli*: a review', *Crit. Rev. Biotechnol.*, vol. 40, no. 4, pp. 475–489, May 2020, doi: 10.1080/07388551.2020.1742646.
- [8] L.-N. Schaffert and W. G. Carter, 'Do Post-Translational Modifications Influence Protein Aggregation in Neurodegenerative Diseases: A Systematic Review', *Brain Sci.*, vol. 10, no. 4, p. 232, Apr. 2020, doi: 10.3390/brainsci10040232.
- [9] J. A. Raskatov and D. B. Teplow, 'Using chirality to probe the conformational dynamics and assembly of intrinsically disordered amyloid proteins', *Sci. Rep.*, vol. 7, no. 1, p. 12433, Dec. 2017, doi: 10.1038/s41598-017-10525-5.
- [10] C. M. Dobson, 'Protein folding and misfolding', *Nature*, vol. 426, no. 6968, pp. 884–890, Dec. 2003, doi: 10.1038/nature02261.
- [11] F. U. Hartl, A. Bracher, and M. Hayer-Hartl, 'Molecular chaperones in protein folding and proteostasis', *Nature*, vol. 475, no. 7356, pp. 324–332, Jul. 2011, doi: 10.1038/nature10317.
- [12] S. Sharma, P. Modi, G. Sharma, and S. Deep, 'Kinetics theories to understand the mechanism of aggregation of a protein and to design strategies for its inhibition', *Biophys. Chem.*, vol. 278, p. 106665, Nov. 2021, doi: 10.1016/j.bpc.2021.106665.
- [13] M. Nilsson, 'Techniques to study amyloid fibril formation in vitro', *Methods*, vol. 34, no. 1, pp. 151–160, Sep. 2004, doi: 10.1016/j.ymeth.2004.03.012.

- [14] A. W. Fitzpatrick and H. R. Saibil, 'Cryo-EM of amyloid fibrils and cellular aggregates', *Curr. Opin. Struct. Biol.*, vol. 58, pp. 34–42, Oct. 2019, doi: 10.1016/j.sbi.2019.05.003.
- [15] M. Lu, C. F. Kaminski, and G. S. K. Schierle, 'Advanced fluorescence imaging of in situ protein aggregation', *Phys. Biol.*, vol. 17, no. 2, p. 021001, Mar. 2020, doi: 10.1088/1478-3975/ab694e.
- [16] M. Lu *et al.*, 'Live-cell super-resolution microscopy reveals a primary role for diffusion in polyglutamine-driven aggresome assembly', *J. Biol. Chem.*, vol. 294, no. 1, pp. 257–268, Jan. 2019, doi: 10.1074/jbc.RA118.003500.
- [17] M. Beasley, S. Groover, S. J. Valentine, and J. Legleiter, 'Lipid headgroups alter huntingtin aggregation on membranes', *Biochim. Biophys. Acta BBA - Biomembr.*, vol. 1863, no. 1, p. 183497, Jan. 2021, doi: 10.1016/j.bbamem.2020.183497.
- [18] M. Beasley, N. Frazee, S. Groover, S. J. Valentine, B. Mertz, and J. Legleiter, 'Physicochemical Properties Altered by the Tail Group of Lipid Membranes Influence Huntingtin Aggregation and Lipid Binding', *J. Phys. Chem. B*, vol. 126, no. 16, pp. 3067–3081, Apr. 2022, doi: 10.1021/acs.jpcc.1c10254.
- [19] P. Frid, S. V. Anisimov, and N. Popovic, 'Congo red and protein aggregation in neurodegenerative diseases', *Brain Res. Rev.*, vol. 53, no. 1, pp. 135–160, Jan. 2007, doi: 10.1016/j.brainresrev.2006.08.001.
- [20] K. M. Batzli and B. J. Love, 'Agitation of amyloid proteins to speed aggregation measured by ThT fluorescence: A call for standardization', *Mater. Sci. Eng. C*, vol. 48, pp. 359–364, Mar. 2015, doi: 10.1016/j.msec.2014.09.015.
- [21] C. Xue, T. Y. Lin, D. Chang, and Z. Guo, 'Thioflavin T as an amyloid dye: fibril quantification, optimal concentration and effect on aggregation', *R. Soc. Open Sci.*, vol. 4, no. 1, p. 160696, Jan. 2017, doi: 10.1098/rsos.160696.
- [22] R. Khurana *et al.*, 'Mechanism of thioflavin T binding to amyloid fibrils', *J. Struct. Biol.*, vol. 151, no. 3, pp. 229–238, Sep. 2005, doi: 10.1016/j.jsb.2005.06.006.
- [23] M. Biancalana and S. Koide, 'Molecular mechanism of Thioflavin-T binding to amyloid fibrils', *Biochim. Biophys. Acta BBA - Proteins Proteomics*, vol. 1804, no. 7, pp. 1405–1412, Jul. 2010, doi: 10.1016/j.bbapap.2010.04.001.
- [24] C. Wu, Z. Wang, H. Lei, W. Zhang, and Y. Duan, 'Dual Binding Modes of Congo Red to Amyloid Protofibril Surface Observed in Molecular Dynamics Simulations', *J. Am. Chem. Soc.*, vol. 129, no. 5, pp. 1225–1232, Feb. 2007, doi: 10.1021/ja0662772.
- [25] C. Xue, T. Y. Lin, D. Chang, and Z. Guo, 'Thioflavin T as an amyloid dye: fibril quantification, optimal concentration and effect on aggregation', *R. Soc. Open Sci.*, vol. 4, no. 1, p. 160696, Jan. 2017, doi: 10.1098/rsos.160696.
- [26] P. McColgan and S. J. Tabrizi, 'Huntington's disease: a clinical review', *Eur. J. Neurol.*, vol. 25, no. 1, pp. 24–34, Jan. 2018, doi: 10.1111/ene.13413.

- [27] R. Ghosh and S. J. Tabrizi, 'Clinical Features of Huntington's Disease', in *Polyglutamine Disorders*, vol. 1049, C. Nóbrega and L. Pereira de Almeida, Eds. Cham: Springer International Publishing, 2018, pp. 1–28. doi: 10.1007/978-3-319-71779-1_1.
- [28] C. A. Ross and S. J. Tabrizi, 'Huntington's disease: from molecular pathogenesis to clinical treatment', *Lancet Neurol.*, vol. 10, no. 1, pp. 83–98, Jan. 2011, doi: 10.1016/S1474-4422(10)70245-3.
- [29] C. Zühlke, O. Rless, B. Bockel, H. Lange, and U. Thies, 'Mitotic stability and meiotic variability of the (CAG)_n repeat in the Huntington disease gene', *Hum. Mol. Genet.*, vol. 2, no. 12, pp. 2063–2067, 1993, doi: 10.1093/hmg/2.12.2063.
- [30] J. B. Penney *et al.*, 'Huntington's disease in venezuela: 7 years of follow-up on symptomatic and asymptomatic individuals', *Mov. Disord.*, vol. 5, no. 2, pp. 93–99, 1990, doi: 10.1002/mds.870050202.
- [31] J. G. Hodgson *et al.*, 'A YAC Mouse Model for Huntington's Disease with Full-Length Mutant Huntingtin, Cytoplasmic Toxicity, and Selective Striatal Neurodegeneration', *Neuron*, vol. 23, no. 1, pp. 181–192, May 1999, doi: 10.1016/S0896-6273(00)80764-3.
- [32] S. Chen, F. A. Ferrone, and R. Wetzel, 'Huntington's disease age-of-onset linked to polyglutamine aggregation nucleation', *Proc. Natl. Acad. Sci.*, vol. 99, no. 18, pp. 11884–11889, Sep. 2002, doi: 10.1073/pnas.182276099.
- [33] G. Stuitje *et al.*, 'Age of onset in Huntington's disease is influenced by CAG repeat variations in other polyglutamine disease-associated genes', *Brain*, vol. 140, no. 7, pp. e42–e42, Jul. 2017, doi: 10.1093/brain/awx122.
- [34] K. J. Wyant, A. J. Ridder, and P. Dayalu, 'Huntington's Disease—Update on Treatments', *Curr. Neurol. Neurosci. Rep.*, vol. 17, no. 4, p. 33, Apr. 2017, doi: 10.1007/s11910-017-0739-9.
- [35] E. Kayson *et al.*, 'The Prospective Huntington At-Risk Observational Study (PHAROS): The Emotional Well-Being, Safety and Feasibility of Long-Term Research Participation', p. 7.
- [36] J. S. Paulsen, K. F. Hoth, C. Nehl, L. Stierman, and The Huntington Study Group, 'Critical Periods of Suicide Risk in Huntington's Disease', *Am. J. Psychiatry*, vol. 162, no. 4, pp. 725–731, Apr. 2005, doi: 10.1176/appi.ajp.162.4.725.
- [37] J. S. Paulsen, 'Cognitive Impairment in Huntington Disease: Diagnosis and Treatment', *Curr. Neurol. Neurosci. Rep.*, vol. 11, no. 5, pp. 474–483, Oct. 2011, doi: 10.1007/s11910-011-0215-x.
- [38] K. F. Hoth, J. S. Paulsen, D. J. Moser, D. Tranel, L. A. Clark, and A. Bechara, 'Patients with Huntington's disease have impaired awareness of cognitive, emotional, and functional abilities', *J. Clin. Exp. Neuropsychol.*, vol. 29, no. 4, pp. 365–376, May 2007, doi: 10.1080/13803390600718958.
- [39] J. F. Gusella, M. E. MacDonald, and J.-M. Lee, 'Genetic modifiers of Huntington's disease: GENETIC MODIFIERS OF HD', *Mov. Disord.*, vol. 29, no. 11, pp. 1359–1365, Sep. 2014, doi: 10.1002/mds.26001.
- [40] R. L. Margolis and C. A. Ross, 'Diagnosis of Huntington Disease', *Clin. Chem.*, vol. 49, no. 10, pp. 1726–1732, Oct. 2003, doi: 10.1373/49.10.1726.

- [41] R. Dorsey *et al.*, 'Use of Tetrabenazine in Huntington Disease Patients on Antidepressants or with Advanced Disease: Results from the TETRA-HD Study', *PLoS Curr.*, vol. 3, p. RRN1283, Nov. 2011, doi: 10.1371/currents.RRN1283.
- [42] C. Rinaldi and M. J. A. Wood, 'Antisense oligonucleotides: the next frontier for treatment of neurological disorders', *Nat. Rev. Neurol.*, vol. 14, no. 1, pp. 9–21, Jan. 2018, doi: 10.1038/nrneurol.2017.148.
- [43] E. J. Wild and S. J. Tabrizi, 'Therapies targeting DNA and RNA in Huntington's disease', *Lancet Neurol.*, vol. 16, no. 10, pp. 837–847, Oct. 2017, doi: 10.1016/S1474-4422(17)30280-6.
- [44] C. M. Sousa and S. Humbert, 'Huntingtin: Here, There, Everywhere!', p. 9.
- [45] S. L. Crick, K. M. Ruff, K. Garai, C. Frieden, and R. V. Pappu, 'Unmasking the roles of N- and C-terminal flanking sequences from exon 1 of huntingtin as modulators of polyglutamine aggregation', *Proc. Natl. Acad. Sci.*, vol. 110, no. 50, pp. 20075–20080, Dec. 2013, doi: 10.1073/pnas.1320626110.
- [46] F. Saudou and S. Humbert, 'The Biology of Huntingtin', *Neuron*, vol. 89, no. 5, pp. 910–926, Mar. 2016, doi: 10.1016/j.neuron.2016.02.003.
- [47] I. S. Seong *et al.*, 'Huntingtin facilitates polycomb repressive complex 2', *Hum. Mol. Genet.*, vol. 19, no. 4, pp. 573–583, Feb. 2010, doi: 10.1093/hmg/ddp524.
- [48] W. Li, L. C. Serpell, W. J. Carter, D. C. Rubinsztein, and J. A. Huntington, 'Expression and Characterization of Full-length Human Huntingtin, an Elongated HEAT Repeat Protein', *J. Biol. Chem.*, vol. 281, no. 23, pp. 15916–15922, Jun. 2006, doi: 10.1074/jbc.M511007200.
- [49] H. Takano and J. F. Gusella, 'The predominantly HEAT-like motif structure of huntingtin and its association and coincident nuclear entry with dorsal, an NF- κ B/Rel/dorsal family transcription factor', *BMC Neurosci.*, p. 13, 2002.
- [50] J. R. Arndt, M. Chaibva, and J. Legleiter, 'The emerging role of the first 17 amino acids of huntingtin in Huntington's disease', *Biomol. Concepts*, vol. 6, no. 1, pp. 33–46, Mar. 2015, doi: 10.1515/bmc-2015-0001.
- [51] M. P. Duyao *et al.*, 'Inactivation of the Mouse Huntington's Disease Gene Homolog *Hdh*', *Science*, vol. 269, no. 5222, pp. 407–410, Jul. 1995, doi: 10.1126/science.7618107.
- [52] E. Colin *et al.*, 'Huntingtin phosphorylation acts as a molecular switch for anterograde/retrograde transport in neurons', *EMBO J.*, vol. 27, no. 15, pp. 2124–2134, Aug. 2008, doi: 10.1038/emboj.2008.133.
- [53] J. P. Caviston, J. L. Ross, S. M. Antony, M. Tokito, and E. L. F. Holzbaur, 'Huntingtin facilitates dynein/dynactin-mediated vesicle transport', *Proc. Natl. Acad. Sci.*, vol. 104, no. 24, pp. 10045–10050, Jun. 2007, doi: 10.1073/pnas.0610628104.
- [54] F. Gasset-Rosa *et al.*, 'Polyglutamine-Expanded Huntingtin Exacerbates Age-Related Disruption of Nuclear Integrity and Nucleocytoplasmic Transport', *Neuron*, vol. 94, no. 1, pp. 48-57.e4, Apr. 2017, doi: 10.1016/j.neuron.2017.03.027.

- [55] K. Sathasivam *et al.*, 'Aberrant splicing of HTT generates the pathogenic exon 1 protein in Huntington disease', *Proc. Natl. Acad. Sci.*, vol. 110, no. 6, pp. 2366–2370, Feb. 2013, doi: 10.1073/pnas.1221891110.
- [56] E. L. Bunting, J. Hamilton, and S. J. Tabrizi, 'Polyglutamine diseases', *Curr. Opin. Neurobiol.*, vol. 72, pp. 39–47, Feb. 2022, doi: 10.1016/j.conb.2021.07.001.
- [57] A. K. Thakur *et al.*, 'Polyglutamine disruption of the huntingtin exon 1 N terminus triggers a complex aggregation mechanism', *Nat. Struct. Mol. Biol.*, vol. 16, no. 4, pp. 380–389, Apr. 2009, doi: 10.1038/nsmb.1570.
- [58] A. Bhattacharyya *et al.*, 'Oligoproline Effects on Polyglutamine Conformation and Aggregation', *J. Mol. Biol.*, vol. 355, no. 3, pp. 524–535, Jan. 2006, doi: 10.1016/j.jmb.2005.10.053.
- [59] M. Chen and P. G. Wolynes, 'Aggregation landscapes of Huntingtin exon 1 protein fragments and the critical repeat length for the onset of Huntington's disease', *Proc. Natl. Acad. Sci.*, vol. 114, no. 17, pp. 4406–4411, Apr. 2017, doi: 10.1073/pnas.1702237114.
- [60] D. W. Colby *et al.*, 'Potent inhibition of huntingtin aggregation and cytotoxicity by a disulfide bond-free single-domain intracellular antibody', *Proc. Natl. Acad. Sci.*, vol. 101, no. 51, pp. 17616–17621, Dec. 2004, doi: 10.1073/pnas.0408134101.
- [61] S. Vieweg, A. Ansaloni, Z.-M. Wang, J. B. Warner, and H. A. Lashuel, 'An Intein-based Strategy for the Production of Tag-free Huntingtin Exon 1 Proteins Enables New Insights into the Polyglutamine Dependence of Httex1 Aggregation and Fibril Formation', *J. Biol. Chem.*, vol. 291, no. 23, pp. 12074–12086, Jun. 2016, doi: 10.1074/jbc.M116.713982.
- [62] S. Chen, 'Solubilization and disaggregation of polyglutamine peptides', *Protein Sci.*, vol. 10, no. 4, pp. 887–891, Apr. 2001, doi: 10.1110/ps.42301.
- [63] A. Reif, A. Chiki, J. Ricci, and H. A. Lashuel, 'Generation of Native, Untagged Huntingtin Exon1 Monomer and Fibrils Using a SUMO Fusion Strategy', *J. Vis. Exp.*, no. 136, p. 57506, Jun. 2018, doi: 10.3791/57506.
- [64] P. Shemella *et al.*, 'Mechanism for Intein C-Terminal Cleavage: A Proposal from Quantum Mechanical Calculations', *Biophys. J.*, vol. 92, no. 3, pp. 847–853, Feb. 2007, doi: 10.1529/biophysj.106.092049.
- [65] P. Guedes-Dias and E. L. F. Holzbaur, 'Huntingtin Fibrils Poke Membranes', *Cell*, vol. 171, no. 1, pp. 32–33, Sep. 2017, doi: 10.1016/j.cell.2017.09.009.
- [66] D. T. W. Chang, G. L. Rintoul, S. Pandipati, and I. J. Reynolds, 'Mutant huntingtin aggregates impair mitochondrial movement and trafficking in cortical neurons', *Neurobiol. Dis.*, vol. 22, no. 2, pp. 388–400, May 2006, doi: 10.1016/j.nbd.2005.12.007.
- [67] K. A. Burke, E. A. Yates, and J. Legleiter, 'Biophysical Insights into How Surfaces, Including Lipid Membranes, Modulate Protein Aggregation Related to Neurodegeneration', *Front. Neurol.*, vol. 4, 2013, doi: 10.3389/fneur.2013.00017.

- [68] X. Gao *et al.*, 'Cholesterol Modifies Huntingtin Binding to, Disruption of, and Aggregation on Lipid Membranes', *Biochemistry*, vol. 55, no. 1, pp. 92–102, Jan. 2016, doi: 10.1021/acs.biochem.5b00900.
- [69] K. A. Burke, K. M. Hensal, C. S. Umbaugh, M. Chaibva, and J. Legleiter, 'Huntingtin disrupts lipid bilayers in a polyQ-length dependent manner', *Biochim. Biophys. Acta BBA - Biomembr.*, vol. 1828, no. 8, pp. 1953–1961, Aug. 2013, doi: 10.1016/j.bbamem.2013.04.025.
- [70] M. Tao, N. K. Pandey, R. Barnes, S. Han, and R. Langen, 'Structure of Membrane-Bound Huntingtin Exon 1 Reveals Membrane Interaction and Aggregation Mechanisms', *Structure*, vol. 27, no. 10, pp. 1570-1580.e4, Oct. 2019, doi: 10.1016/j.str.2019.08.003.
- [71] K. A. Burke, K. J. Kauffman, C. S. Umbaugh, S. L. Frey, and J. Legleiter, 'The Interaction of Polyglutamine Peptides with Lipid Membranes Is Regulated by Flanking Sequences Associated with Huntingtin', *J. Biol. Chem.*, vol. 288, no. 21, pp. 14993–15005, May 2013, doi: 10.1074/jbc.M112.446237.
- [72] G. Scanavachi, A. Coutinho, A. A. Fedorov, M. Prieto, A. M. Melo, and R. Itri, 'Lipid Hydroperoxide Compromises the Membrane Structure Organization and Softens Bending Rigidity', *Langmuir*, vol. 37, no. 33, pp. 9952–9963, Aug. 2021, doi: 10.1021/acs.langmuir.1c00830.
- [73] R. S. Hilgarth and K. D. Sarge, 'Detection of Sumoylated Proteins', in *Ubiquitin-Proteasome Protocols*, vol. 301, New Jersey: Humana Press, 2005, pp. 329–338. doi: 10.1385/1-59259-895-1:329.
- [74] M. Wördehoff and W. Hoyer, 'α-Synuclein Aggregation Monitored by Thioflavin T Fluorescence Assay', *BIO-Protoc.*, vol. 8, no. 14, 2018, doi: 10.21769/BioProtoc.2941.
- [75] M. Sebastiao, N. Quittot, and S. Bourgault, 'Thioflavin T fluorescence to analyse amyloid formation kinetics: Measurement frequency as a factor explaining irreproducibility', *Anal. Biochem.*, vol. 532, pp. 83–86, Sep. 2017, doi: 10.1016/j.ab.2017.06.007.
- [76] A. Sulatskaya *et al.*, 'Investigation of α-Synuclein Amyloid Fibrils Using the Fluorescent Probe Thioflavin T', *Int. J. Mol. Sci.*, vol. 19, no. 9, p. 2486, Aug. 2018, doi: 10.3390/ijms19092486.
- [77] C. Carmo, L. Naia, C. Lopes, and A. C. Rego, 'Mitochondrial Dysfunction in Huntington's Disease', in *Polyglutamine Disorders*, vol. 1049, C. Nóbrega and L. Pereira de Almeida, Eds. Cham: Springer International Publishing, 2018, pp. 59–83. doi: 10.1007/978-3-319-71779-1_3.
- [78] M. L. Duennwald, S. Jagadish, P. J. Muchowski, and S. Lindquist, 'Flanking sequences profoundly alter polyglutamine toxicity in yeast', *Proc. Natl. Acad. Sci.*, vol. 103, no. 29, pp. 11045–11050, Jul. 2006, doi: 10.1073/pnas.0604547103.
- [79] A. Urbanek *et al.*, 'Flanking Regions Determine the Structure of the Poly-Glutamine in Huntingtin through Mechanisms Common among Glutamine-Rich Human Proteins', *Structure*, vol. 28, no. 7, pp. 733-746.e5, Jul. 2020, doi: 10.1016/j.str.2020.04.008.
- [80] M. Birol and A. M. Melo, 'Untangling the Conformational Polymorphism of Disordered Proteins Associated With Neurodegeneration at the Single-Molecule Level', *Front. Mol. Neurosci.*, vol. 12, p. 309, Jan. 2020, doi: 10.3389/fnmol.2019.00309.

- [81] A. K. Karanji, M. Beasley, D. Sharif, A. Ranjbaran, J. Legleiter, and S. J. Valentine, 'Investigating the interactions of the first 17 amino acid residues of Huntingtin with lipid vesicles using mass spectrometry and molecular dynamics', *J. Mass Spectrom.*, vol. 55, no. 1, Jan. 2020, doi: 10.1002/jms.4470.